PERGAMON

International Journal of Hydrogen Energy 27 (2002) 301–322

International Journal of HYDROGEN ENERGY

www.elsevier.com/locate/ijhydene

Spectral emission of fractional quantum energy levels of atomic hydrogen from a helium–hydrogen plasma and the implications for dark matter

Randell L. Mills *, Paresh Ray

BlackLight Power, Inc., 493 Old Trenton Road, Cranbury, NJ 08512, USA

Abstract

From a solution of a Schrödinger-type wave equation with a nonradiative boundary condition based on Maxwell's equations, Mills predicts that atomic hydrogen may undergo a catalytic reaction with certain atomized elements and ions which singly or multiply ionize at integer multiples of the potential energy of atomic hydrogen, $m27.2$ eV wherein m is an integer. The reaction involves a nonradiative energy transfer to form a hydrogen atom that is lower in energy than unreacted atomic hydrogen that corresponds to a fractional principal quantum number ($n = 1/p = 1/\text{integer}$ replaces the well-known parameter $n = \text{integer}$ in the Rydberg equation for hydrogen excited states). One such atomic catalytic system involves helium ions. The second ionization energy of helium is 54.4 eV; thus, the ionization reaction of He^+ to He^{2+} has a net enthalpy of reaction of 54.4 eV which is equivalent to 2×27.2 eV. Since the products of the catalysis reaction have binding energies of $m27.2$ eV, they may further serve as catalysts. Extreme ultraviolet (EUV) spectroscopy was recorded on microwave and glow discharges of helium with 2% hydrogen. Novel emission lines were observed with energies of $q13.6$ eV where $q = 1, 2, 3, 4, 6, 7, 8, 9,$ *or* 11 or these lines inelastically scattered by helium atoms wherein 21.2 eV was absorbed in the excitation of He ($1s^2$) to He ($1s^1 2p^1$). These lines were identified as hydrogen transitions to electronic energy levels below the "ground" state corresponding to fractional quantum numbers. Furthermore, astrophysical data was reviewed and such transitions were found to match certain spectral lines of the extreme ultraviolet background of interstellar space. They may resolve the paradox of the identity of dark matter and account for many celestial observations such as: diffuse Hα emission is ubiquitous throughout the Galaxy and widespread sources of flux shortward of 912 Å are required. Fractional hydrogen transitions were also assigned to unidentified lines in the solar EUV spectrum which may resolve the solar neutrino problem, the mystery of the cause of sunspots and other solar activity, and why the Sun emits X-rays.

1. Introduction

1.1. Background

J. J. Balmer showed in 1885 that the frequencies for some of the lines observed in the emission spectrum of atomic hydrogen could be expressed with a completely empirical relationship. This approach was later extended by J. R. Rydberg, who showed that all of the spectral lines of atomic hydrogen were given by the equation

$$\tilde{\nu} = R\left(\frac{1}{n_f^2} - \frac{1}{n_i^2}\right), \tag{1}$$

where $R = 109,677\ \text{cm}^{-1}$, $n_f = 1, 2, 3, \ldots$, $n_i = 2, 3, 4, \ldots$, and $n_i > n_f$.

Niels Bohr, in 1913, developed a theory for atomic hydrogen that gave energy levels in agreement with Rydberg's equation. An identical equation, based on a totally

* Corresponding author. Tel.: +1-609-490-1090; fax: +1-609-490-1066.

E-mail address: rmills@blacklightpower.com (R.L. Mills).

0360-3199/02/$ 20.00
PII: S0360-3199(01)00116-1

different theory for the hydrogen atom, was developed by E. Schrödinger, and independently by W. Heisenberg, in 1926.

$$E_n = -\frac{e^2}{n^2 8\pi\varepsilon_0 a_H} = -\frac{13.598\ \text{eV}}{n^2}, \tag{2a}$$

$$n = 1, 2, 3, \ldots, \tag{2b}$$

where a_H is the Bohr radius for the hydrogen atom (52.947 pm), e is the magnitude of the charge of the electron, and ε_0 is the vacuum permittivity. Based on the solution of a Schrödinger-type wave equation with a nonradiative boundary condition based on Maxwell's equations, Mills [1–41] predicts that atomic hydrogen may undergo a catalytic reaction with certain atomized elements or certain gaseous ions which singly or multiply ionize at integer multiples of the potential energy of atomic hydrogen, 27.2 eV. The reaction involves a nonradiative energy transfer to form a hydrogen atom that is lower in energy than unreacted atomic hydrogen that corresponds to a fraction principal quantum number where Eq. (2b), should be replaced by Eq. (2c).

$$n = 1, 2, 3, \ldots \quad \text{and} \quad n = \frac{1}{2}, \frac{1}{3}, \frac{1}{4}, \ldots . \tag{2c}$$

A number of independent experimental observations lead to the conclusion that atomic hydrogen can exist in fractional quantum states that are at lower energies than the traditional "ground" ($n = 1$) state.

1.2. Experimental data of lower-energy hydrogen

Observation of intense extreme ultraviolet (EUV) emission at low temperatures (e.g. $\approx 10^3$ K) from atomic hydrogen and certain atomized elements or certain gaseous ions [7–24] has been reported previously. The only pure elements that were observed to emit EUV were those wherein the ionization of t electrons from an atom to a continuum energy level is such that the sum of the ionization energies of the t electrons is approximately $m27.2$ eV where t and m are each an integer. Potassium, cesium, and strontium atoms and Rb^+ ion ionize at integer multiples of the potential energy of atomic hydrogen and caused emission. Whereas, the chemically similar atoms, sodium, magnesium and barium, do not ionize at integer multiples of the potential energy of atomic hydrogen and caused no emission.

Prior studies that support the possibility of a novel reaction of atomic hydrogen which produces a chemically generated or assisted plasma, fractional-principal-quantum-energy-level hydrogen atoms, molecules, and hydride ions, and novel hydride compounds include extreme ultraviolet (EUV) spectroscopy [7–9,11–24], plasma formation [7–24], power generation [10–12,17,25], and analysis of chemical compounds [8,9,20,22–39]. Exemplary studies include:

(1) The recent analysis of mobility and spectroscopy data of individual electrons in liquid helium which shows direct experimental confirmation that electrons may have fractional principal quantum energy levels [6].

(2) The observation of continuum state emission of Cs^{2+} and Ar^{2+} at 533 and 456 Å, respectively, with the absence of the other corresponding Rydberg series of lines from these species which confirmed the resonant nonradiative energy transfer of 27.2 eV from atomic hydrogen to the catalysts atomic Cs or Ar^+ [9].

(3) The spectroscopic observation of the predicted hydride ion $H^-(1/2)$ of hydrogen catalysis by either Cs or Ar^+ catalyst at 4070 Å corresponding to its predicted binding energy of 3.05 eV [9].

(4) The observation of characteristic emission from K^{3+} which confirmed the resonant nonradiative energy transfer of 3×27.2 eV from atomic hydrogen to atomic potassium [8].

(5) The spectroscopic observation of the predicted $H^-(1/4)$ hydride ion of hydrogen catalysis by potassium catalyst at 1100 Å corresponding to its predicted binding energy of 11.2 eV [8].

(6) The identification of transitions of atomic hydrogen to lower-energy levels corresponding to fractional principal quantum numbers in the extreme ultraviolet emission spectrum from interstellar medium [1,5].

(7) The EUV spectroscopic observation of lines by the Institut für Niedertemperatur-Plasmaphysik e.V. that could be assigned to transitions of atomic hydrogen to lower-energy levels corresponding to fractional principal quantum numbers and the emission from the excitation of the corresponding hydride ions [14].

(8) The observation of novel EUV emission lines from microwave discharges of argon or helium with 10% hydrogen that matched those predicted for vibrational transitions of H_2^* $[n = 1/4; n^* = 2]^+$ with energies of $v1.185$ eV, $v = 17$–38 that terminated at the predicted dissociation limit, E_D, of H_2 $[n = 1/4]^+$, $E_D = 42.88$ eV (28.92 nm) [7].

(9) The observation by the Institut für Niedertemperatur-Plasmaphysik e.V. of an anomalous plasma and plasma afterglow duration formed with hydrogen–potassium mixtures [15].

(10) The observation of anomalous afterglow durations of plasmas formed by catalysts providing a net enthalpy of reaction within thermal energies of $m27.28$ eV [15,16].

(11) The observation of Lyman series in the EUV that represents an energy release 10 times hydrogen combustion which is greater than that of any possible known chemical reaction [8–24].

(12) The observation of line emission by the Institut für Niedertemperatur-Plasmaphysik e.V. with a 4° grazing incidence EUV spectrometer that was 100 times more energetic than the combustion of hydrogen [14].

(13) The observation of anomalous plasmas formed with strontium and argon catalysts at 1% of the theoretical or prior known voltage requirement with a light output for power input up to 8600 times that of the control standard light source [11,12,17].

(14) The observation that the optically measured output power of gas cells for power supplied to the glow discharge increased by over two orders of magnitude depending on the presence of less than 1% partial pressure of certain catalysts in hydrogen gas or argon–hydrogen gas mixtures [10].
(15) The isolation of novel hydrogen compounds as products of the reaction of atomic hydrogen with atoms and ions which formed an anomalous plasma as reported in the EUV studies [20,22–39].
(16) The identification of novel hydride compounds by (i) time of flight secondary ion mass spectroscopy which showed a dominant hydride ion in the negative ion spectrum, (ii) X-ray photoelectron spectroscopy which showed novel hydride peaks and significant shifts of the core levels of the primary elements bound to the novel hydride ions, (iii) ^{1}H nuclear magnetic resonance spectroscopy (NMR) which showed extraordinary upfield chemical shifts compared to the NMR of the corresponding ordinary hydrides, and (iv) thermal decomposition with analysis by gas chromatography, and mass spectroscopy which identified the compounds as hydrides [20,22–39].
(17) The NMR identification of novel hydride compounds MH^*X wherein M is the metal, X, is a halide, and H^* comprises a novel high binding energy hydride ion identified by a large distinct upfield resonance [25,26,29].
(18) The replication of the NMR results of the identification of novel hydride compounds by large distinct upfield resonances at Spectral Data Services, University of Massachusetts Amherst, University of Delaware, Grace Davison, and National Research Council of Canada [25].
(19) The NMR identification of novel hydride compounds MH^* and MH_2^* wherein M is the metal and H^* comprises a novel high binding energy hydride ion identified by a large distinct upfield resonance that proves the hydride ion is different from the hydride ion of the corresponding known compound of the same composition [25].
(20) The differential scanning calorimetry (DSC) measurement of minimum heats of formation of KHI by the catalytic reaction of potassium with atomic hydrogen and KI that were over -2000 kJ (mol H_2)$^{-1}$ compared to the enthalpy of combustion of hydrogen of -241.8 kJ (mol H_2)$^{-1}$ [39].

1.3. Mechanism of the formation of lower-energy hydrogen

The mechanism of EUV emission, formation of novel hydrides, and certain EUV lines from interstellar medium cannot be explained by the conventional energy levels of hydrogen, but it is predicted by a solution of the Schrödinger equation with a nonradiative boundary constraint put forward by Mills [1]. Mills predicts that certain atoms or ions serve as catalysts to release energy from hydrogen to produce an increased binding energy hydrogen atom called a *hydrino atom* having a binding energy given by Eq. (2a) where

$$n = \frac{1}{2}, \frac{1}{3}, \frac{1}{4}, \ldots, \frac{1}{p} \tag{3}$$

and p is an integer greater than 1, designated as $H[a_H/p]$ where a_H is the radius of the hydrogen atom. Hydrinos are predicted to form by reacting an ordinary hydrogen atom with a catalyst having a net enthalpy of reaction of about

$$m27.2 \text{ eV}, \tag{4}$$

where m is an integer. This catalysis releases energy from the hydrogen atom with a commensurate decrease in size of the hydrogen atom, $r_n = na_H$. For example, the catalysis of $H(n = 1)$ to $H(n = 1/2)$ releases 40.8 eV, and the hydrogen radius decreases from a_H to $1/2a_H$.

The excited energy states of atomic hydrogen are also given by Eq. (2a) except with Eq. (2b). The $n = 1$ state is the "ground" state for "pure" photon transitions (the $n = 1$ state can absorb a photon and go to an excited electronic state, but it cannot release a photon and go to a lower-energy electronic state). However, an electron transition from the ground state to a lower-energy state is possible by a nonradiative energy transfer such as multipole coupling or a resonant collision mechanism. These lower-energy states have fractional quantum numbers, $n = 1/\text{integer}$. Processes that occur without photons and that require collisions are common. For example, the exothermic chemical reaction of $H + H$ to form H_2 does not occur with the emission of a photon. Rather, the reaction requires a collision with a third body, M, to remove the bond energy — $H + H + M \rightarrow H_2 + M^*$ [42]. The third body distributes the energy from the exothermic reaction, and the end result is the H_2 molecule and an increase in the temperature of the system.

Some commercial phosphors are based on nonradiative energy transfer involving multipole coupling. For example, the strong absorption strength of Sb^{3+} ions along with the efficient nonradiative transfer of excitation from Sb^{3+} to Mn^{2+}, are responsible for the strong manganese luminescence from phosphors containing these ions [43].

Similarly, the $n = 1$ state of hydrogen and the $n = 1/\text{integer}$ states of hydrogen are nonradiative, but a transition between two nonradiative states is possible via a nonradiative energy transfer, say $n = 1$ to $1/2$. In these cases, during the transition the electron couples to another electron transition, electron transfer reaction, or inelastic scattering reaction which can absorb the exact amount of energy that must be removed from the hydrogen atom to cause the transition. Thus, a catalyst provides a net positive enthalpy of reaction of $m27.2$ eV (i.e. it absorbs $m27.2$ eV where m is an integer). Certain atoms or ions serve as catalysts which resonantly accept energy from hydrogen atoms and release the energy to the surroundings to effect electronic transitions to fractional quantum energy levels.

The catalysis of hydrogen involves the nonradiative transfer of energy from atomic hydrogen to a catalyst which may then release the transferred energy by radiative and nonradiative mechanisms. As a consequence of the nonradiative energy transfer, the hydrogen atom becomes unstable and emits further energy until it achieves a lower-energy nonradiative state having a principal energy level given by Eqs. (2a) and (3).

1.4. Catalysts

1.4.1. Helium ion

Helium ion (He^+) is such a catalyst because the second ionization energy of helium is 54.417 eV, which is equivalent to $m = 2$ in Eq. (4). In this case, the catalysis reaction is

$$54.417\ \text{eV} + He^+ + H[a_H] \rightarrow He^{2+} + e^- + H\left[\frac{a_H}{3}\right] + 108.8\ \text{eV}, \quad (5)$$

$$He^{2+} + e^- \rightarrow He^+ + 54.417\ \text{eV} \quad (6)$$

and, the overall reaction is

$$H[a_H] \rightarrow H\left[\frac{a_H}{3}\right] + 54.4\ \text{eV} + 54.4\ \text{eV}. \quad (7)$$

The energy given off during catalysis is much greater than the energy lost to the catalyst. The energy released is large as compared to conventional chemical reactions. For example, when hydrogen and oxygen gases undergo combustion to form water

$$H_2(g) + \frac{1}{2}O_2(g) \rightarrow H_2O(l) \quad (8)$$

the known enthalpy of formation of water is $\Delta H_f = -286\ \text{kJ mol}^{-1}$ or 1.48 eV per hydrogen atom. By contrast, each ($n = 1$) ordinary hydrogen atom undergoing catalysis releases a net of 108.8 eV. Moreover, further catalytic transitions may occur: $n = \frac{1}{3} \rightarrow \frac{1}{4}, \frac{1}{4} \rightarrow \frac{1}{5}$, and so on. Once catalysis begins, hydrinos autocatalyze further in a process called *disproportionation*. This mechanism is similar to that of an inorganic ion catalysis. But, hydrino catalysis should have a higher reaction rate than that of the inorganic ion catalyst due to the better match of the enthalpy to $m27.2$ eV.

1.4.2. Hydrino catalysts

In a process called *disproportionation*, lower-energy hydrogen atoms, *hydrinos*, can act as catalysts because each of the metastable excitation, resonance excitation, and ionization energy of a hydrino atom is $m27.2$ eV (Eq. (4)). The transition reaction mechanism of a first hydrino atom affected by a second hydrino atom involves the resonant coupling between the atoms of m degenerate multipoles each having 27.21 eV of potential energy [1]. The energy transfer of $m27.2$ eV from the first hydrino atom to the second hydrino atom causes the central field of the first atom to increase by m and its electron to drop m levels lower from a radius of a_H/p to a radius of $a_H/(p+m)$. The second interacting lower-energy hydrogen is either excited to a metastable state, excited to a resonance state, or ionized by the resonant energy transfer. The resonant transfer may occur in multiple stages. For example, a nonradiative transfer by multipole coupling may occur wherein the central field of the first increases by m, then the electron of the first drops m levels lower from a radius of a_H/p to a radius of $a_H/(p+m)$ with further resonant energy transfer. The energy transferred by multipole coupling may occur by a mechanism that is analogous to photon absorption involving an excitation to a virtual level. Or, the energy transferred by multipole coupling during the electron transition of the first hydrino atom may occur by a mechanism that is analogous to two photon absorption involving a first excitation to a virtual level and a second excitation to a resonant or continuum level [44–46]. The transition energy greater than the energy transferred to the second hydrino atom may appear as a photon in a vacuum medium.

The transition of $H[a_H/p]$ to $H[a_H/(p+m)]$ induced by a multipole resonance transfer of $m27.21$ eV (Eq. (4)) and a transfer of $[(p')^2 - (p'-m')^2]13.6\ \text{eV} - m27.2$ eV with a resonance state of $H[a_H/(p'-m')]$ excited in $H[a_H/p']$ is represented by

$$H\left[\frac{a_H}{p'}\right] + H\left[\frac{a_H}{p}\right] \rightarrow H\left[\frac{a_H}{(p'-m')}\right] + H\left[\frac{a_H}{(p+m)}\right] + [((p+m)^2 - p^2) - (p'^2 - (p'-m')^2)]13.6\ \text{eV}, \quad (9)$$

where p, p', m, and m' are integers.

Hydrinos may be ionized during a disproportionation reaction by the resonant energy transfer. A hydrino atom with the initial lower-energy state quantum number p and radius a_H/p may undergo a transition to the state with lower-energy state quantum number $(p+m)$ and radius $a_H/(p+m)$ by reaction with a hydrino atom with the initial lower-energy state quantum number m', initial radius a_H/m', and final radius a_H that provides a net enthalpy of $m27.2$ eV (Eq. (4)). Thus, reaction of hydrogen-type atom, $H[a_H/p]$, with the hydrogen-type atom, $H[a_H/m']$, that is ionized by the resonant energy transfer to cause a transition reaction is represented by

$$m27.21\ \text{eV} + H\left[\frac{a_H}{m'}\right] + H\left[\frac{a_H}{p}\right] \rightarrow H^+ + e^- + H\left[\frac{a_H}{(p+m)}\right] + [(p+m)^2 - p^2 - (m'^2 - 2m)]13.6\ \text{eV}, \quad (10)$$

$$H^+ + e^- \rightarrow H\left[\frac{a_H}{1}\right] + 13.6\ \text{eV}. \quad (11)$$

and, the overall reaction is

$$H\left[\frac{a_H}{m'}\right] + H\left[\frac{a_H}{p}\right] \rightarrow H\left[\frac{a_H}{1}\right] + H\left[\frac{a_H}{(p+m)}\right] + [2pm + m^2 - m'^2]13.6 + 13.6\ \text{eV}. \quad (12)$$

Helium ion catalyzes $H[a_H]$ to $H[a_H/3]$ as shown in Eqs. (5)–(7). Further disproportionation reactions may then proceed

$$H\left[\frac{a_H}{3}\right] + H\left[\frac{a_H}{3}\right] \rightarrow H\left[\frac{a_H}{4}\right] + H\left[\frac{a_H}{2}\right] + 27.2\ \text{eV}, \quad (13)$$

$$H[a_H] + H\left[\frac{a_H}{2}\right] \rightarrow H\left[\frac{a_H}{3}\right] + H^+ + e^- + 54.4\ \text{eV}, \quad (14)$$

$$H\left[\frac{a_H}{2}\right] + H\left[\frac{a_H}{2}\right] \rightarrow H\left[\frac{a_H}{3}\right] + H^+ + e^- + 13.6\ \text{eV}, \quad (15)$$

$$H\left[\frac{a_H}{2}\right] + H\left[\frac{a_H}{2}\right] \rightarrow H\left[\frac{a_H}{3}\right] + H[a_H] + 27.2\ \text{eV}, \quad (16)$$

$$H\left[\frac{a_H}{2}\right] + H\left[\frac{a_H}{2}\right] \rightarrow H\left[\frac{a_H}{4}\right] + H^+ + e^- + 108.8\ \text{eV}, \quad (17)$$

$$H\left[\frac{a_H}{2}\right] + H\left[\frac{a_H}{2}\right] \rightarrow H\left[\frac{a_H}{4}\right] + H[a_H] + 122.4\ \text{eV}, \quad (18)$$

$$H\left[\frac{a_H}{3}\right] + H\left[\frac{a_H}{2}\right] \rightarrow H\left[\frac{a_H}{4}\right] + H^+ + e^- + 40.8\ \text{eV}, \quad (19)$$

$$H\left[\frac{a_H}{3}\right] + H\left[\frac{a_H}{2}\right] \rightarrow H\left[\frac{a_H}{4}\right] + H[a_H] + 54.4\ \text{eV}, \quad (20)$$

$$H\left[\frac{a_H}{4}\right] + H\left[\frac{a_H}{2}\right] \rightarrow H\left[\frac{a_H}{5}\right] + H^+ + e^- + 68\ \text{eV}, \quad (21)$$

$$H\left[\frac{a_H}{4}\right] + H\left[\frac{a_H}{2}\right] \rightarrow H\left[\frac{a_H}{5}\right] + H[a_H] + 81.6\ \text{eV}, \quad (22)$$

$$H\left[\frac{a_H}{2}\right] + He^+ \rightarrow H\left[\frac{a_H}{4}\right] + He^{2+} + e^- + 108.8\ \text{eV}, \quad (23)$$

$$H[a_H] + H\left[\frac{a_H}{3}\right] \rightarrow H\left[\frac{a_H}{4}\right] + H^+ + e^- + 81.6\ \text{eV}, \quad (24)$$

$$H\left[\frac{a_H}{3}\right] + H\left[\frac{a_H}{3}\right] \rightarrow H\left[\frac{a_H}{5}\right] + H\left[\frac{a_H}{2}\right] + 149.6\ \text{eV}, \quad (25)$$

$$H\left[\frac{a_H}{3}\right] + H\left[\frac{a_H}{3}\right] \rightarrow H\left[\frac{a_H}{5}\right] + H[a_H] + 108.8\ \text{eV}, \quad (26)$$

$$H\left[\frac{a_H}{3}\right] + H\left[\frac{a_H}{3}\right] \rightarrow H\left[\frac{a_H}{5}\right] + H^+ + e^- + 95.2\ \text{eV}, \quad (27)$$

$$H\left[\frac{a_H}{4}\right] + H\left[\frac{a_H}{3}\right] \rightarrow H\left[\frac{a_H}{5}\right] + H\left[\frac{a_H}{2}\right] + 54.4\ \text{eV}, \quad (28)$$

$$H\left[\frac{a_H}{4}\right] + H\left[\frac{a_H}{3}\right] \rightarrow H\left[\frac{a_H}{5}\right] + H[a_H] + 13.6\ \text{eV}, \quad (29)$$

$$H\left[\frac{a_H}{5}\right] + H\left[\frac{a_H}{2}\right] \rightarrow H\left[\frac{a_H}{6}\right] + H^+ + e^- + 95.2\ \text{eV}, \quad (30)$$

$$H\left[\frac{a_H}{5}\right] + H\left[\frac{a_H}{2}\right] \rightarrow H\left[\frac{a_H}{6}\right] + H[a_H] + 108.8\ \text{eV}, \quad (31)$$

$$H\left[\frac{a_H}{6}\right] + H\left[\frac{a_H}{2}\right] \rightarrow H\left[\frac{a_H}{7}\right] + H^+ + e^- + 122.4\ \text{eV}, \quad (32)$$

$$H\left[\frac{a_H}{6}\right] + H\left[\frac{a_H}{2}\right] \rightarrow H\left[\frac{a_H}{7}\right] + H[a_H] + 136\ \text{eV}, \quad (33)$$

$$H\left[\frac{a_H}{7}\right] + H\left[\frac{a_H}{2}\right] \rightarrow H\left[\frac{a_H}{8}\right] + H^+ + e^- + 149.6\ \text{eV}, \quad (34)$$

$$H\left[\frac{a_H}{7}\right] + H\left[\frac{a_H}{2}\right] \rightarrow H\left[\frac{a_H}{8}\right] + H[a_H] + 163.2\ \text{eV}. \quad (35)$$

1.4.3. Inelastic scattering by atomic helium

It is proposed that the photons that arise from hydrogen catalysis may undergo inelastic helium scattering. That is, the catalytic reaction

$$H[a_H] \xrightarrow{He} H\left[\frac{a_H}{3}\right] + 54.4 + 54.4\ \text{eV} \quad (36)$$

yields two 54.4 eV photons (228 Å). When each of these photons strikes He ($1s^2$), 21.2 eV is absorbed in the excitation to He ($1s^1 2p^1$). This leaves a 33.19 eV (374 Å) photon peak shown in Table 1. Thus, for helium the inelastic scattered peak of 54.4 eV photons from Eqs. (7), (14), (20), and (28) is given by

$$E = 54.4 - 21.21\ \text{eV} = 33.19\ \text{eV}\ (374\ \text{Å}). \quad (37)$$

For helium, the inelastic scattered peak of 27.2 eV photons from Eqs. (13) and (16) is given by

$$E = 27.2 - 21.21\ \text{eV} = 5.99\ \text{eV}\ (2071\ \text{Å}). \quad (38)$$

Table 1
Observed line emission from helium–hydrogen plasmas assigned to the disproportionation reactions given by Eqs. (9)–(12) and helium inelastic scattered peaks of hydrogen transitions, wherein the photon strikes He ($1s^2$) and 21.2 eV is absorbed in the excitation to He ($1s^1 2p^1$)

Observed line (Å)	Predicted (Mills) (Å)	Assignment (Mills)	Equation no.	Figures
82.9	82.9	$H\left[\frac{a_H}{3}\right] + H\left[\frac{a_H}{3}\right] \rightarrow H\left[\frac{a_H}{5}\right] + H\left[\frac{a_H}{2}\right] + 149.6\ eV$,	(25)	12
		$H\left[\frac{a_H}{7}\right] + H\left[\frac{a_H}{2}\right] \rightarrow H\left[\frac{a_H}{8}\right] + H^+ + e^- + 149.6\ eV$,	(34)	
101.3	101.3	$H\left[\frac{a_H}{2}\right] + H\left[\frac{a_H}{2}\right] \rightarrow H\left[\frac{a_H}{4}\right] + H[a_H] + 122.4\ eV$,	(18)	12
		$H\left[\frac{a_H}{6}\right] + H\left[\frac{a_H}{2}\right] \rightarrow H\left[\frac{a_H}{7}\right] + H^+ + e^- + 122.4\ eV$,	(32)	
130.3[a]	130.3	$H\left[\frac{a_H}{3}\right] + H\left[\frac{a_H}{3}\right] \rightarrow H\left[\frac{a_H}{5}\right] + H^+ + e^- + 95.2\ eV$,	(27)	12
		$H\left[\frac{a_H}{5}\right] + H\left[\frac{a_H}{2}\right] \rightarrow H\left[\frac{a_H}{6}\right] + H^+ + e^- + 95.2\ eV$,	(30)	
141.5	141.5	$H\left[\frac{a_H}{2}\right] + H\left[\frac{a_H}{2}\right] \rightarrow H\left[\frac{a_H}{4}\right] + H^+ + e^- + 108.8\ eV$,	(17)	12
		$H\left[\frac{a_H}{2}\right] + He^+ \rightarrow H\left[\frac{a_H}{4}\right] + He^{2+} + e^- + 108.8\ eV$,	(23)	
		$H\left[\frac{a_H}{3}\right] + H\left[\frac{a_H}{3}\right] \rightarrow H\left[\frac{a_H}{5}\right] + H[a_H] + 108.8\ eV$,	(26)	
		$H\left[\frac{a_H}{5}\right] + H\left[\frac{a_H}{2}\right] \rightarrow H\left[\frac{a_H}{6}\right] + H[a_H] + 108.8\ eV$,	(31)	
		$108.8\ eV + He\ (1s^2) \rightarrow He\ (1s^1 2p^1) \rightarrow +87.59\ eV$,	(43)	
205	205	$H\left[\frac{a_H}{4}\right] + H\left[\frac{a_H}{2}\right] \rightarrow H\left[\frac{a_H}{5}\right] + H[a_H] + 81.6\ eV$,	(22)	7, 8, 9, 10, 12
		$H[a_H] + H\left[\frac{a_H}{3}\right] \rightarrow H\left[\frac{a_H}{4}\right] + H^+ + e^- + 81.6\ eV$,	(24)	
		$81.6\ eV + He\ (1s^2) \rightarrow He\ (1s^1 2p^1) \rightarrow +60.39\ eV$,	(41)	
304	304	$H\left[\frac{a_H}{3}\right] + H\left[\frac{a_H}{2}\right] \rightarrow H\left[\frac{a_H}{4}\right] + H^+ + e^- + 40.8\ eV$,	(19)	7, 8, 9, 10, 12
304	304	$He^+\ (n=2) \rightarrow He^+\ (n=1) + 40.8\ eV$[b],		7, 8, 9, 10, 12
374	374	$H[a_H] \xrightarrow{He^+} H\left[\frac{a_H}{3}\right] + 54.4 + 54.4\ eV$,	(5)–(7)	7, 8, 9, 10, 12
		$H[a_H] + H\left[\frac{a_H}{2}\right] \rightarrow H\left[\frac{a_H}{3}\right] + H^+ + e^- + 54.4\ eV$,	(14)	
		$H\left[\frac{a_H}{3}\right] + H\left[\frac{a_H}{2}\right] \rightarrow H\left[\frac{a_H}{4}\right] + H[a_H] + 54.4\ eV$,	(20)	
		$H\left[\frac{a_H}{4}\right] + H\left[\frac{a_H}{3}\right] \rightarrow H\left[\frac{a_H}{5}\right] + H\left[\frac{a_H}{2}\right] + 54.4\ eV$,	(28)	
		$54.4\ eV + He\ (1s^2) \rightarrow He\ (1s^1 2p^1) \rightarrow +33.19\ eV$,	(37)	
456	456	$H\left[\frac{a_H}{3}\right] + H\left[\frac{a_H}{3}\right] \rightarrow H\left[\frac{a_H}{4}\right] + H\left[\frac{a_H}{2}\right] + 27.2\ eV$,	(13)	7, 8, 9, 10, 12
		$H\left[\frac{a_H}{2}\right] + H\left[\frac{a_H}{2}\right] \rightarrow H\left[\frac{a_H}{3}\right] + H[a_H] + 27.2\ eV$,	(16)	
584	584	$He\ (1s^1 2p^1) \rightarrow He\ (1s^2) + 21.2\ eV$[c],		6, 7, 10, 13
633	633	$H\left[\frac{a_H}{3}\right] + H\left[\frac{a_H}{2}\right] \rightarrow H\left[\frac{a_H}{4}\right] + H^{+} + e^- + 40.8\ eV$,	(19)	13
		$40.8\ eV + He\ (1s^2) \rightarrow He\ (1s^1 2p^1) \rightarrow +19.59\ eV$,	(39)	
633	633	$He^-\ (n=2) \rightarrow He^+\ (n=1) + 40.8\ eV$[b],		13
		$40.8\ eV + He\ (1s^2) \rightarrow He\ (1s^1 2p^1) \rightarrow +19.59\ eV$,	(39)	

Table. 1 (*continued*).

Observed line (Å)	Predicted (Mills) (Å)	Assignment (Mills)	Equation no.	Figures
912	912	$H\left[\frac{a_H}{2}\right] + H\left[\frac{a_H}{2}\right] \rightarrow H\left[\frac{a_H}{3}\right] + H^+ + e^- + 13.6\,eV$,	(15)	14
		$H\left[\frac{a_H}{4}\right] + H\left[\frac{a_H}{3}\right] \rightarrow H\left[\frac{a_H}{5}\right] + H[a_H] + 13.6\,eV$,	(29)	
912	912	$H^+ + e^- \rightarrow H[a_H] + 13.6\,eV$[d].		15

[a]Weak shoulder on the 141.5 Å peak.

[b]In Figs. 7–10, and 12, the peak corresponding to He^+ ($n = 3$) — He^+ ($n = 1$) + 48.35 eV (256 Å) was absent which makes this assignment difficult.

[c]The intensity which is off-scale in Fig. 13 as 56,771 photons/s; thus, the transition He ($1s^2$) — He ($1s^1 2p^1$) dominated the inelastic scattering of EUV peaks.

[d]The ratio of the Lβ peak to the 912 Å peak of the helium–hydrogen plasma shown in Fig. 14 was 2; whereas, the ratio of the Lβ peak to the 912 Å peak of the control hydrogen plasma shown in Fig. 15, was 8 which makes this assignment difficult.

For helium, the inelastic scattered peak of 40.8 eV photons from Eq. (19) is given by

$$E = 40.8 - 21.21\ eV = 19.59\ eV\ (633\ Å). \quad (39)$$

For helium, the inelastic scattered peak of 68 eV photons from Eq. (21) is given by

$$E = 68 - 21.21\ eV = 46.79\ eV\ (265\ Å). \quad (40)$$

For helium, the inelastic scattered peak of 81.6 eV photons from Eqs. (22) and (24) is given by

$$E = 81.6 - 21.21\ eV = 60.39\ eV\ (205\ Å). \quad (41)$$

For helium, the inelastic scattered peak of 95.2 eV photons from Eqs. (27) and (30) is given by

$$E = 95.2 - 21.21\ eV = 73.99\ eV\ (167.6\ Å). \quad (42)$$

For helium, the inelastic scattered peak of 108.8 eV photons from Eqs. (17), (23), (26), and (31) is given by

$$E = 108.8 - 21.21\ eV = 87.59\ eV\ (141.6\ Å). \quad (43)$$

1.5. EUV spectroscopy detects lower-energy hydrogen

Previously reported lines observed at the Institut für Niedertemperatur-Plasmaphysik e.V. by EUV spectroscopy could be assigned to transitions of atomic hydrogen to lower-energy levels corresponding to hydrinos and the emission from the excitation of the corresponding hydride ions [14]. For example, the product of the catalysis of atomic hydrogen with potassium metal, $H[a_H/4]$, may serve as both a catalyst and a reactant to form $H[a_H/3]$ and $H[a_H/6]$. The transition of $H[a_H/4]$ to $H[a_H/6]$ induced by a multipole resonance transfer of 54.4 eV (2 × 27.2 eV) and a transfer of 40.8 eV with a resonance state of $H[a_H/3]$ excited in $H[a_H/4]$ is represented by

$$H\left[\frac{a_H}{4}\right] + H\left[\frac{a_H}{4}\right] - H\left[\frac{a_H}{6}\right] + H\left[\frac{a_H}{3}\right] + 176.8\ eV. \quad (44)$$

The predicted 176.8 eV (70.2 Å) photon is a close match with the observed 73.0 Å line. The energy of this line emission corresponds to an equivalent temperature of 1,000,000°C and an energy over 100 times the energy of combustion of hydrogen.

Since the sun and stars contain significant amounts of He^+ and atomic hydrogen, catalysis of atomic hydrogen by He^+ as given by Eqs. (5)–(7) may occur. Also, the simultaneous ionization of two hydrogen atoms may provide a net enthalpy given by Eq. (4) to catalyze hydrino formation. Once formed, hydrinos have binding energies given by Eqs. (2a) and (3); thus, they may serve as reactants which provide a net enthalpy of reaction given by Eq. (4). Characteristic emissions from the Sun corresponding to these reactions may be observed, and stellar production may be a source of hydrinos in interstellar space where further transitions may occur with corresponding emission of characteristic EUV lines.

The detection of atomic hydrogen in fractional quantum energy levels below the traditional "ground" state — hydrinos — was previously reported [1,5] by the assignment of soft X-ray emissions from the interstellar medium, the Sun, and stellar flares, and by assignment of certain lines obtained by the far-infrared absolute spectrometer (FIRAS) on the cosmic background explorer. The detection of a new molecular species — the diatomic hydrino molecule — was reported by the assignment of certain infrared line emissions from the Sun. The detection of a new hydride species — hydrino hydride ion — was reported by the assignment of certain soft X-ray, ultraviolet (UV), and visible emissions from the Sun. This has implications for several unresolved astrophysical problems such as the identity of dark matter and the solar neutrino paradox.

We report that extreme ultraviolet (EUV) spectroscopy was recorded on microwave and glow discharges of helium with 2% hydrogen. Novel emission lines were observed with energies of $q13.6$ eV where $q = 1, 2, 3, 4, 6, 7, 8, 9$, *or* 11 or these lines inelastically scattered by helium atoms wherein 21.2 eV was absorbed in the excitation of He($1s^2$) to He ($1s^1 2p^1$). These lines were identified as hydrogen transitions to electronic energy levels below the "ground" state corresponding to fractional quantum numbers. A comparison was made between the plasma results and astrophysical data. Similar lower-energy-hydrogen transitions were found that matched the spectral lines of the extreme ultraviolet background of interstellar space and solar lines.

2. Experimental

2.1. EUV spectroscopy

Extreme ultraviolet (EUV) spectroscopy was recorded on microwave and discharge cell light sources. Due to the extremely short wavelength of this radiation, "transparent" optics do not exist. Therefore, a windowless arrangement was used wherein the microwave or discharge cell was connected to the same vacuum vessel as the grating and detectors of the extreme ultraviolet (EUV) spectrometer. Differential pumping permitted a high pressure in the cell as compared to that in the spectrometer. This was achieved by pumping on the cell outlet and pumping on the grating side of the collimator that served as a pin-hole inlet to the optics. The spectrometer was continuously evacuated to 10^{-4}–10^{-6} Torr by a turbomolecular pump with the pressure read by a cold cathode pressure gauge. The EUV spectrometer was connected to the cell light source with a 1.5 mm × 5 mm collimator which provided a light path to the slits of the EUV spectrometer. The collimator also served as a flow constrictor of gas from the cell. The cell was operated under gas flow conditions while maintaining a constant gas pressure in the cell.

Spectra were obtained on hydrogen, helium, and xenon (not a catalyst in this system) and mixtures of 2% hydrogen with helium, neon, or xenon. The noble gas–hydrogen mixtures (98/2%) were made from ultrahigh purity gases by addition of hydrogen to the noble gas to achieve a 98/2% mixture based on the individual gas partial pressures.

For spectral measurement, the light emission from microwave plasmas of hydrogen alone, helium–hydrogen (98/2%), and neon–hydrogen (98/2%), and light emission from a discharge plasma of hydrogen alone were introduced to a normal incidence McPherson 0.2 meter monochromator (Model 302, Seya-Namioka type) equipped with a 1200 lines/mm holographic grating with a platinum coating. The wavelength region covered by the monochromator was 50–5600 Å. The EUV spectrum was recorded with a channel electron multiplier (CEM) at 2500–3000 V. The wavelength resolution was about 0.2 Å (FWHM) with an entrance and exit slit width of 50 μm. The increment was 2 Å and the dwell time was 500 ms.

To achieve higher sensitivity at the shorter EUV wavelengths, the light emission of control microwave plasmas of hydrogen alone, helium alone, and glow discharge plasmas of hydrogen, xenon, helium–hydrogen mixture (98/2%), and xenon–hydrogen mixture (98/2%) were recorded with a McPherson 4° grazing incidence EUV spectrometer (Model 248/310G) equipped with a grating having 600 G/mm with a radius of curvature of ≈ 1 m. The angle of incidence was 87°. The wavelength region covered by the monochromator was 50–650 Å. The wavelength resolution was about 0.4 Å (FWHM) with an entrance and exit slit width of 300 μm. A CEM at 2400 V was used to detect the EUV light. The increment was 1 Å and the dwell time was 1 s.

2.2. Microwave emission spectra

The experimental set up comprising a microwave discharge gas cell light source and an EUV spectrometer which was differentially pumped is shown in Fig. 1. Extreme ultraviolet emission spectra were obtained on plasmas of hydrogen alone, helium alone, helium–hydrogen mixture (98/2%), and neon–hydrogen mixture (98/2%) with a microwave discharge system and an EUV spectrometer. The microwave generator was a Opthos model MPG-4M generator (Frequency: 2450 MHz). The input power was set at 85 W. Helium–hydrogen (98/2%) gas mixture was flowed through a half-inch diameter quartz tube at 1, 20, or 760 Torr. The gas pressure inside the cell was maintained by flowing the mixture while monitoring the pressure with a 10 and 1000 Torr MKS Baratron absolute pressure gauge. By the same method, hydrogen alone plasmas were run at 1 and 20 Torr, and plasmas of helium alone and neon–hydrogen mixture (98/2%) were run at 20 Torr. The tube was fitted with an Opthos coaxial microwave cavity (Evenson cavity). The EUV spectrometer was a normal incidence monochromator except for the helium alone plasma and an additional hydrogen alone plasma which were recorded with a 4° grazing incidence EUV spectrometer (see Section 2.1).

2.3. Glow discharge emission spectra

A diagram of the discharge plasma source is given in Fig. 2. The hollow cathode and EUV spectrograph were aligned on a common optical axis using a laser. The experimental setup for the discharge measurements is illustrated in Fig. 3. Extreme ultraviolet emission spectra were obtained on plasmas of hydrogen, xenon, helium–hydrogen mixture (98/2%), and xenon–hydrogen mixture (98/2%) with a gas discharge cell that comprised a five-way stainless-steel cross that served as the anode with a hollow stainless-steel cathode. The plasma was generated at the hollow cathode inside the discharge cell. The hollow cathode was constructed of a stainless-steel rod inserted into a steel tube, and this assembly was inserted into an alumina tube. A flange opposite the end of the hollow cathode connected the spectrometer

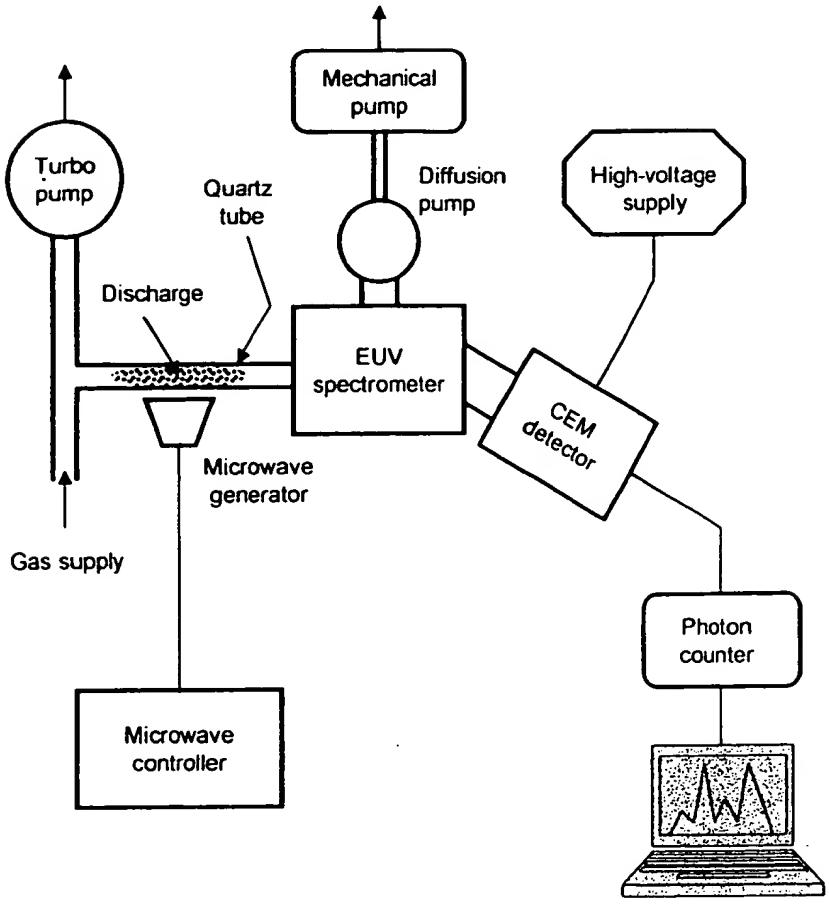

Fig. 1. The experimental set up comprising a microwave discharge gas cell light source and an EUV spectrometer which was differentially pumped.

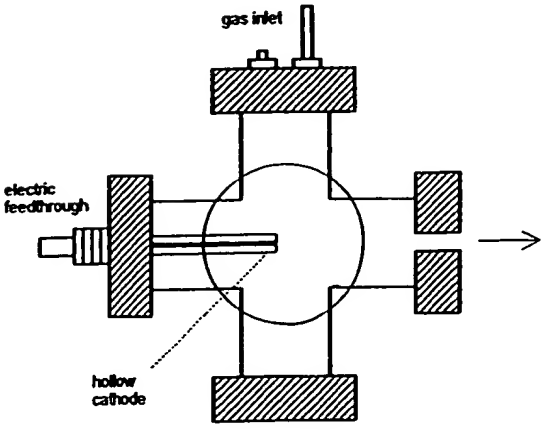

Fig. 2. Cross-sectional view of the discharge cell.

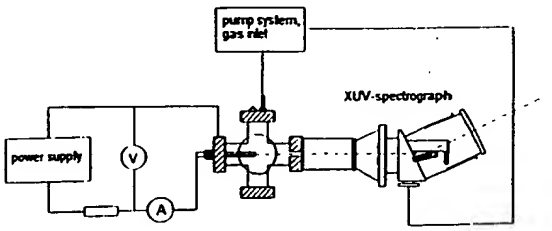

Fig. 3. The experimental set up comprising a discharge gas cell light source and an EUV spectrometer which was differentially pumped.

with the cell. It had a small hole that permitted radiation to pass to the spectrometer. An AC power supply ($V = 0$–1 kV, $I = 0$–100 mA) was connected to the hollow cathode to generate a discharge. The AC voltage and current at the time the EUV spectrum was recorded were 200 V and 40 mA, respectively. A Swagelok adapter at the very

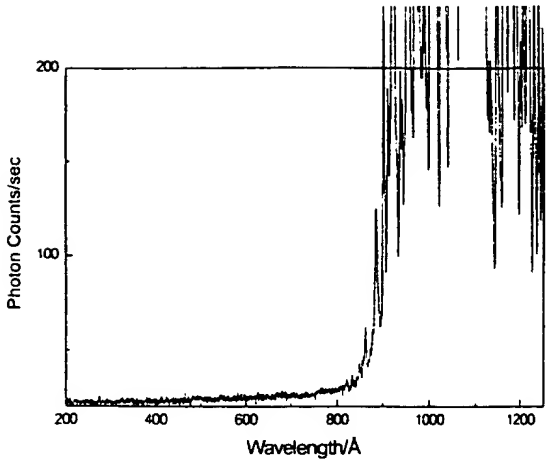

Fig. 4. The EUV spectrum (200–1250 Å) of the control hydrogen discharge cell emission that was recorded with a normal incidence EUV spectrometer and a CEM. No emission was observed below 800 Å.

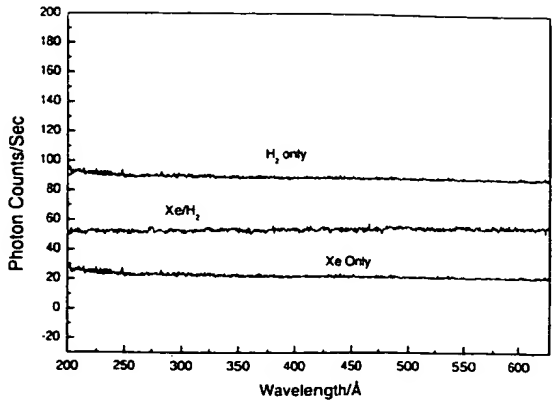

Fig. 5. The EUV spectra (200–645 Å) of the control hydrogen (top curve), control xenon–hydrogen mixture (98/2%) (middle curve), and control xenon (bottom curve) discharge cell emission that were recorded with a 4° grazing incidence EUV spectrometer and a CEM. No peaks were observed in this region from xenon alone or with the addition of hydrogen. No instrument artifacts were observed.

end of the steel cross provided a gas inlet and a connection with the pumping system, and the cell was pumped with a mechanical pump. Valves were between the cell and the mechanical pump, the cell and the monochromator, and the monochromator and its turbo pump. The five-way cross was pressurized with 400 mTorr of gas which was maintained by flowing the gas while monitoring the pressure with a 1 Torr MKS Baratron absolute pressure gauge. The spectrometer was a 4° grazing incidence EUV spectrometer except for an additional hydrogen alone plasma which was recorded with a normal incidence monochromator (see Section 2.1).

3. Results and discussion

3.1. EUV spectroscopy

The EUV emission was recorded from microwave and glow discharge plasmas of hydrogen, helium, and xenon, and helium, neon, and xenon with 2% hydrogen over the wavelength range 50–1250 Å. The EUV spectrum (200–1250 Å) of the control hydrogen discharge cell emission is shown in Fig. 4. The hydrogen glow discharge and microwave discharge emission recorded with the normal incidence monochrometer and the 4° grazing EUV spectrometer were the same. The EUV spectra (200–645 Å) of the control hydrogen (top curve), control xenon–hydrogen mixture (98/2%) (middle curve), and control xenon (bottom curve) discharge cell emission are shown in Fig. 5. No peaks were observed in this region from xenon alone or with the addition of hydrogen. Thus, xenon did not catalyze hydrogen to give novel peaks, and no spurious peaks or artifacts due to the grating or the spectrometer were observed. The EUV

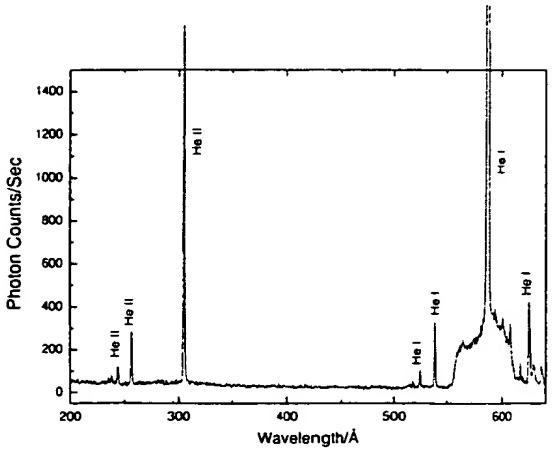

Fig. 6. The EUV spectrum (200–650 Å) of the control helium microwave discharge cell emission that was recorded with a 4° grazing incidence EUV spectrometer and a CEM. Only known He I and He II peaks were observed.

spectrum (200–650 Å) of the control helium microwave cell emission is shown in Fig. 6. Only known He I and He II peaks were observed.

The EUV spectrum (150–650 Å) of the helium–hydrogen mixture (98/2%) microwave cell emission that was recorded at 1, 24, and 72 h is shown in Fig. 7. Ordinary hydrogen has no emission in these regions as shown in Fig. 4. Peaks observed at 205, 374 and 456 Å, which do not correspond to helium and increase with time, were assigned to lower-energy hydrogen transitions in Table 1. A control helium was obtained with the 4° grazing incidence EUV spectrometer since

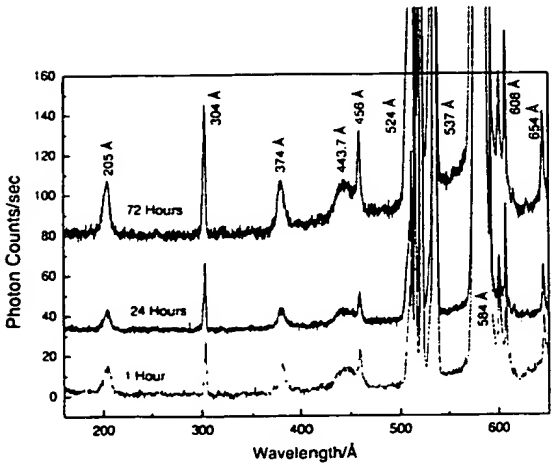

Fig. 7. The EUV spectra (150–650 Å) of the helium–hydrogen mixture (98/2%) microwave cell emission that was recorded at 1, 24, and 72 h with a normal incidence EUV spectrometer and a CEM. The pressure was maintained at 20 Torr. Reproducible novel emission lines that increased with time were observed at 456 and 304 Å with energies of $q13.6$ eV where $q = 2$ *or* 3 and at 374 and 205 Å with energies of $q13.6$ eV where $q = 4$ or 6 that were inelastically scattered by helium atoms wherein 21.2 eV (584 Å) was absorbed in the excitation of He ($1s^2$). These lines were identified in Table 1 as hydrogen transitions to electronic energy levels below the "ground" state corresponding to fractional quantum numbers.

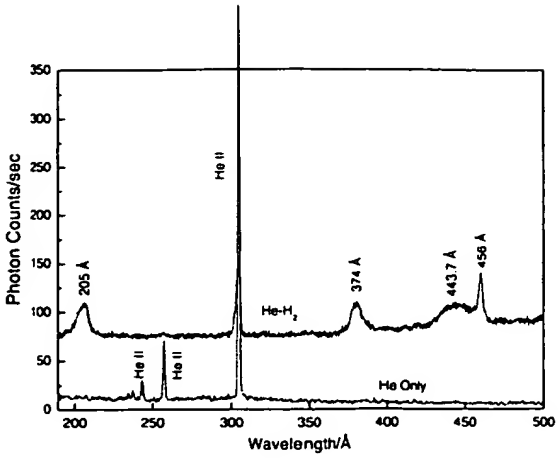

Fig. 8. The EUV spectra (190–500 Å) of the helium–hydrogen mixture (98/2%) (top curve) and control helium (bottom curve) microwave discharge cell emission that were recorded with a normal incidence and a 4° grazing incidence EUV spectrometer, respectively, and a CEM. The lines that corresponded to hydrogen transitions to lower electronic energy levels were not observed in the helium control.

the spectrum with helium alone had very low intensity at the short wavelengths below 584 Å; whereas, the plasma of the helium–hydrogen mixture (98/2%) was much more intense and was obtained on the normal incidence monochromator. The EUV spectra (190–500 Å) of the helium–hydrogen mixture (98/2%) (top curve) and control helium (bottom curve) microwave discharge cell emission is shown in Fig. 8. The lines that corresponded to hydrogen transitions to lower electronic energy levels were not observed in the helium control.

Neon has peaks at 456.35 and 455.27 Å. To eliminate the possibility that the 456 Å peak shown in Fig. 8 was due to the presence of neon as an impurity, the EUV spectra (250–500 Å) of the helium–hydrogen mixture (98/2%) (top curve) and control neon–hydrogen mixture (98/2%) (bottom curve) microwave discharge cell emission were recorded with a normal incidence EUV spectrometer and a CEM as shown in Fig. 9. The lines that corresponded to hydrogen transitions to lower electronic energy levels were not observed in the neon–hydrogen control, and a series of Ne II lines were observed only in the control. The neon peaks at 456.35 and 455.27 Å were resolved in Fig. 9; whereas, the 456 Å peak in the helium–hydrogen plasma was about 30 Å broad. Thus, it was not due to neon impurity.

The pressure was increased from 20 to 760 Torr, and the corresponding spectra were compared in Fig. 10. The

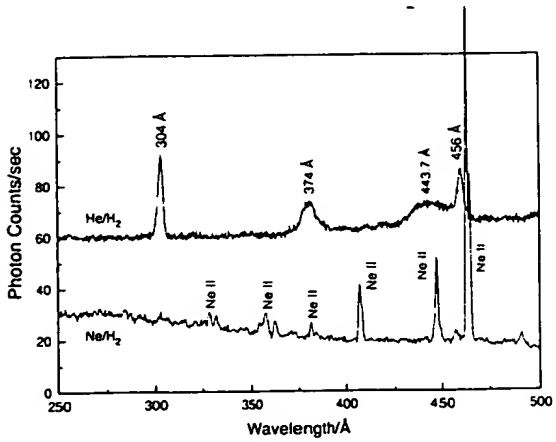

Fig. 9. The EUV spectra (250–500 Å) of the helium–hydrogen mixture (98/2%) (top curve) and control neon–hydrogen mixture (98/2%) (bottom curve) microwave discharge cell emission that were recorded with a normal incidence EUV spectrometer and a CEM. The lines that corresponded to hydrogen transitions to lower electronic energy levels were not observed in the neon–hydrogen control, and a series of Ne II lines were observed only in the control.

peaks appeared slightly more intense at the lower pressure; so, the pressure was decreased to 1 Torr and spectra were recorded. The short-wavelength EUV spectrum (50–600 Å) of the control hydrogen microwave discharge cell emission is shown in Fig. 11. No spectrometer artifacts were observed at the short wavelengths. The short-wavelength EUV spec-

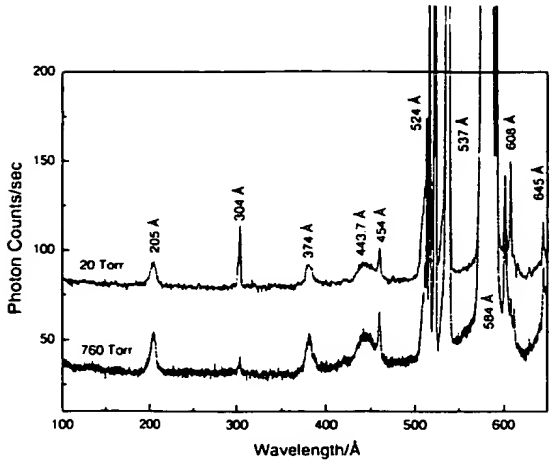

Fig. 10. The EUV spectrum (100–650 Å) of the helium–hydrogen mixture (98/2%) microwave cell emission that was recorded with a normal incidence EUV spectrometer and a CEM. The pressure was maintained at 20 and 760 Torr for the top and bottom curves, respectively. The lines that corresponded to hydrogen transitions to lower electronic energy levels appeared more intense at the lower pressure.

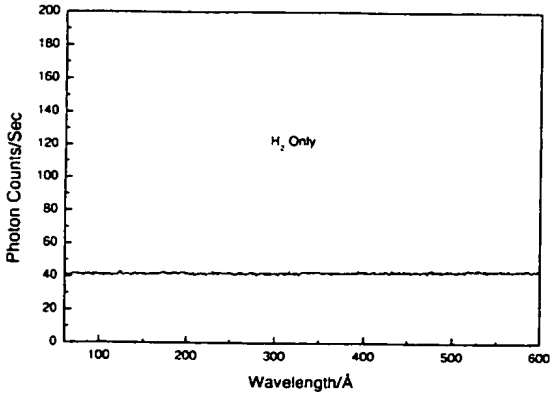

Fig. 11. The short-wavelength EUV spectrum (50–600 Å) of the control hydrogen microwave cell emission that was recorded with a normal incidence EUV spectrometer and a CEM. The pressure was maintained at 1 Torr. No hydrogen emission was observed in this region, and no instrument artifacts were observed.

trum (50–460 Å) of the helium–hydrogen mixture (98/2%) microwave cell emission with a pressure of 1 Torr is shown in Fig. 12. The plasma was the brightest and had an increased background at this condition which is demonstrated by comparison with the control plasma recorded at the same detector sensitivity. At the 1 Torr condition, additional novel peaks were observed in the short-wavelength region. Peaks observed at 82.9, 101.3, 130.3, and 141.5 Å which do not correspond to helium were assigned to lower-energy hydrogen transitions in Table 1. It is also proposed that the 304 Å peak

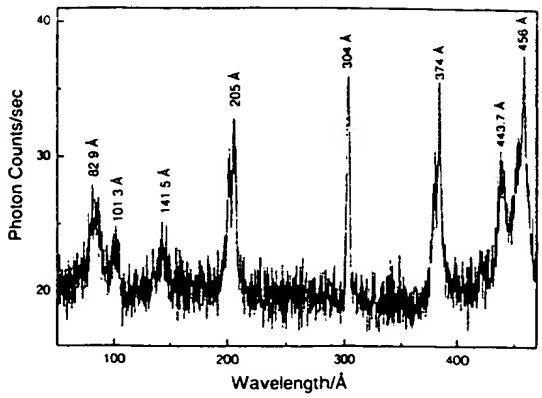

Fig. 12. The short-wavelength EUV spectrum (50–460 Å) of the helium–hydrogen mixture (98/2%) microwave cell emission that was recorded with a normal incidence EUV spectrometer and a CEM. The pressure was maintained at 1 Torr. Reproducible novel emission lines were observed at 456, 304, 130.3, 101.3, and 82.9 Å with energies of $q13.6$ eV where $q = 2$, 3, 7, 9, *or* 11 and at 374, 205, and 141.5 Å with energies of $q13.6$ eV where $q = 4$, 6, *or* 8 that were inelastically scattered by helium atoms wherein 21.2 eV (584 Å) was absorbed in the excitation of He ($1s^2$). These lines were identified in Table 1 as hydrogen transitions to electronic energy levels below the "ground" state corresponding to fractional quantum numbers.

shown in Figs. 7–10 and 12 was not entirely due to the He II transition. Conspicuously absent was the 256 Å (48.3 eV) line of He II shown in Figs. 6 and 8 which implies only a minor He II transition contribution to the 304 Å peak.

The EUV spectrum (500–650 Å) of the helium–hydrogen mixture (98/2%) discharge cell emission is shown in Fig. 13. It is proposed that the 633 Å peak shown in Fig. 13 arises from inelastic helium scattering of the 304 Å peak. That is, the $\frac{1}{3} \rightarrow \frac{1}{4}$ transition yields a 40.8 eV photon (304 Å). When this photon strikes He ($1s^2$), 21.2 eV is absorbed in the excitation to He ($1s^1 2p^1$). This leaves a 19.6 eV (633 Å) photon and a 21.2 eV (584 Å) photon from He ($1s^1 2p^1$). The intensity of the 584 Å shown in Fig. 13 is off-scale with 56.771 photons s^{-1}. Thus, the transition He ($1s^2$) $\rightarrow$ He ($1s^1 2p^1$) dominated the inelastic scattering of EUV peaks. For the first nine peaks assigned as lower-energy hydrogen transitions or such transitions inelastically scattered by helium, the agreement between the predicted values and the experimental values shown in Table 1 is remarkable. It is also remarkable that the hydrino lines are moderately intense based on the low grating efficiency at these short wavelengths.

The EUV spectrum (880–1250 Å) of the helium–hydrogen mixture (98/2%) microwave cell emission is shown in Fig. 14. The EUV spectrum (800–1050 Å) of the control hydrogen microwave cell emission is shown in Fig. 15. The ratio of the Lβ peak to the 912 Å peak of the helium–hydrogen plasma shown in Fig. 14 was 2; whereas,

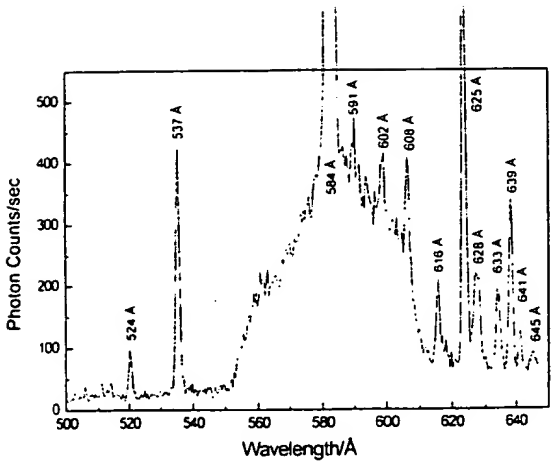

Fig. 13. The EUV spectrum (500–650 Å) of the helium–hydrogen mixture (98/2%) discharge cell emission that was recorded with a 4° grazing incidence EUV spectrometer and a CEM. The pressure was maintained at 400 mTorr. An important astrophysical line was observed at 633 Å corresponding to the 304 Å lower-energy hydrogen transition line shown in Figs. 7–10 and 12 and Table 1 that was inelastically scattered by helium atoms wherein 21.2 eV (584 Å) was absorbed in the excitation of He ($1s^2$).

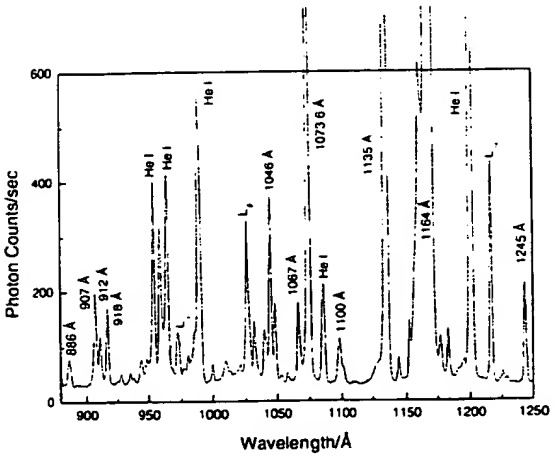

Fig. 14. The EUV spectrum (880–1250 Å) of the helium–hydrogen mixture (98/2%) microwave cell emission that was recorded with a normal incidence EUV spectrometer and a CEM. The pressure was maintained at 20 Torr. An emission line was observed at 912 Å with an energy of $q13.6$ eV where $q = 1$ which was identified in Table 1 as hydrogen transitions to electronic energy levels below the "ground" state corresponding to fractional quantum numbers based on the 912 Å line intensity relative to Lβ compared to that of the control hydrogen plasma.

the ratio of the Lβ peak to the 912 Å peak of the control hydrogen plasma shown in Fig. 15, was 8 which indicates that the majority of the 912 Å peak was due to a transition

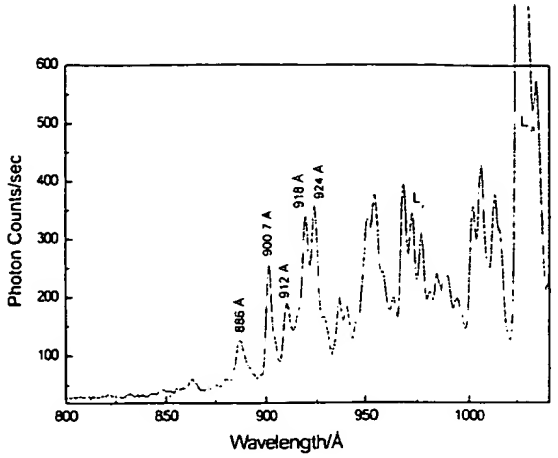

Fig. 15. The EUV spectrum (800–1050 Å) of the control hydrogen microwave discharge cell emission that was recorded with a normal incidence EUV spectrometer and a CEM.

other than the binding of an electron by a proton. Based on the intensity, it is proposed that the majority of the 912 Å peak shown in Fig. 14 was due to the $\frac{1}{2} \rightarrow \frac{1}{4}$ and $\frac{1}{4} \rightarrow \frac{1}{6}$ transitions given in Table 1.

The energies for the hydrogen transitions given in Table 1 in order of energy are 13.6, 27.2, 40.8, 54.4, 81.6, 95.2, 108.8, 122.4 and 149.6 eV. The corresponding peaks are 912, 456, 304 with 633, 374, 205, 130.3, 141.5, 101.3, and 82.9 Å, respectively. Thus, the lines identified in Figs. 7–10 and 12–14 as hydrogen transitions to electronic energy levels below the "ground" state corresponding to fractional quantum numbers correspond to energies of $q13.6$ eV where $q = 1, 2, 3, 4, 6, 7, 8, 9,$ *or* 11 or these lines inelastically scattered by helium atoms wherein 21.2 eV was absorbed in the excitation of He ($1s^2$) to He ($1s^1 2p^1$). The absence of the series members corresponding to $q = 5$ and 10 may be due to a slow reaction rate due to selection rules, low cross-section, or low relative reactant concentrations with only one dominant reaction pathway given by Eqs. (21) and (33), respectively. For example, the data is consistent with the reaction given by Eq. (22) which gives rise to the helium-scattered peak at 205 Å being favored over that given by Eq. (21) corresponding to $q = 5$. And, the reaction cross-section and concentration of $H[a_H/6]$ required in the case of the reaction given by Eq. (33) corresponding to $q = 10$ may have been relatively lower.

The disproportionation reaction assignments given in Table 1 start with the product of the catalysis of atomic hydrogen by He^+ given by Eqs. (5)–(7). One cascade of reactions which gives rise to the peaks assigned in Table 1 is

$$H[a_H] \xrightarrow{He^+} H\left[\frac{a_H}{3}\right] + 54.4 + 54.4 \text{ eV}, \tag{45}$$

$$H\left[\frac{a_H}{3}\right] + H\left[\frac{a_H}{3}\right] \rightarrow H\left[\frac{a_H}{2}\right] + H\left[\frac{a_H}{4}\right] + 27.2\ \text{eV}, \quad (46)$$

$$H\left[\frac{a_H}{2}\right] + H\left[\frac{a_H}{2}\right] \rightarrow H^+ + e^- + H\left[\frac{a_H}{3}\right] + 13.6\ \text{eV}, \quad (47)$$

$$H\left[\frac{a_H}{3}\right] + H\left[\frac{a_H}{2}\right] \rightarrow H^+ + e^- + H\left[\frac{a_H}{4}\right] + 40.8\ \text{eV}, \quad (48)$$

$$H\left[\frac{a_H}{4}\right] + H\left[\frac{a_H}{2}\right] \rightarrow H[a_H] + H\left[\frac{a_H}{5}\right] + 81.6\ \text{eV}, \quad (49)$$

$$H\left[\frac{a_H}{3}\right] + H\left[\frac{a_H}{3}\right] \rightarrow H\left[\frac{a_H}{5}\right] + H^+ + e^- + 95.2\ \text{eV}, \quad (50)$$

$$H\left[\frac{a_H}{3}\right] + H\left[\frac{a_H}{3}\right] \rightarrow H\left[\frac{a_H}{5}\right] + H[a_H] + 108.8\ \text{eV}, \quad (51)$$

$$H\left[\frac{a_H}{2}\right] + H\left[\frac{a_H}{2}\right] \rightarrow H\left[\frac{a_H}{4}\right] + H[a_H] + 122.4\ \text{eV}, \quad (52)$$

$$H\left[\frac{a_H}{3}\right] + H\left[\frac{a_H}{3}\right] \rightarrow H\left[\frac{a_H}{5}\right] + H\left[\frac{a_H}{2}\right] + 149.6\ \text{eV}, \quad (53)$$

wherein peaks inelastically scattered by helium are given by

$$\text{photon}\ (h\nu) + He\ (1s^2) \rightarrow He\ (1s^1 2p^1) + \text{photon}\ (h\nu - 21.21\ \text{eV}). \quad (54)$$

All other peaks besides those assigned to lower-energy hydrogen transitions could be assigned to He I (e.g. 524, 537, 591, 602, 625, 628, 639, 641, 645 Å), He II (assigned in figures), second-order lines (608, 615, 886, 1046, 1073.6, 1135, 1164, 1245 Å), or atomic (e.g. 1216, 1026, 973 Å) or molecular hydrogen (e.g. 907, 918, 1067, 1100 Å) emission [47,48]. No known lines of helium or hydrogen explain the $q13.6$ eV related set of peaks. Given that these spectra are readily repeatable, these peaks may have been overlooked in the past without considering the role of the helium scattering. The 633 Å peak which arises from the helium scattered 304 Å peak has significant astrophysical importance as discussed in the identification of lower-energy hydrogen by soft X-rays from dark interstellar medium section.

3.2. Identification of lower-energy hydrogen by soft X-rays from dark interstellar medium

3.2.1. Dark matter

The universe is predominantly comprised of hydrogen and a small amount of helium. These elements exist in inter stellar regions of space, and they are expected to comprise the majority of interstellar matter. However, the observed constant angular velocity of many galaxies as the distance from the luminous galactic center increases can only be accounted for by the existence of nonluminous weakly interacting matter, dark matter. Dark matter exists at the cold fringes of galaxies and in cold interstellar space. It may account for the majority of the universal mass.

The identity of dark matter has been a cosmological mystery. Postulated assignments include τ neutrinos, but a detailed search for signature emissions has yielded nil [49]. The search for signatures by the cryogenic dark matter search (CDMS) developed to detect theorized weakly interacting massive particles (WIMPs) has similarly yielded nil [50,51]. WIMP theory's main competitor known as MACHO theory which assigns the dark matter to massive compact halo objects (MACHOs) which rather than elusive subatomic particles comprises ordinary baryonic matter in the form of burned-out dark stars, stray planets, and other large, heavy, but dark objects that must be ubiquitous throughout the universe. However, MACHO theory has also recently been ruled out based on lack of evidence of these dark objects observable by the brief ellipses caused by them moving in front of distant stars. Only a few such objects have been observed after exhaustively searching for over five years [50,52].

It is anticipated that the emission spectrum of the extreme ultraviolet background of interstellar matter possesses the spectral signature of dark matter. Labov and Bowyer designed a grazing incidence spectrometer to measure and record the diffuse extreme ultraviolet background [53]. The instrument was carried aboard a sounding rocket, and data were obtained between 80 and 650 Å (data points approximately every 1.5 Å). Several lines including an intense 635 Å emission associated with dark matter were observed [53] which has considerable astrophysical importance as indicated by the authors:

> Regardless of the origin, the 635 Å emission observed could be a major source of ionization. Reynolds (1983, 1984, 1985) has shown that diffuse Hα emission is ubiquitous throughout the Galaxy, and widespread sources of flux shortward of 912 Å are required. Pulsar dispersion measures (Reynolds, 1989) indicate a high scale height for the associated ionized material. Since the path length for radiation shortward of 912 Å is low, this implies that the ionizing source must also have a large scale height and be widespread. Transient heating appears unlikely, and the steady-state ionization rate is more than can be provided by cosmic rays, the soft X-ray background, B stars, or hot white dwarfs (Reynolds, 1986; Brushweiler and Cheng, 1988). Sciama (1990) and Salucci and Sciama (1990) have argued that a variety of observations can be explained by the presence of dark matter in the galaxy which decays with the emission of radiation below 912 Å.

The flux of 635 Å radiation required to produce hydrogen ionization is given by $F = \zeta_{11}/\sigma_\nu = 4.3 \times 10^4 \zeta_{-13}$ photons $cm^{-2}s^{-1}$, where ζ_{-13} is the ionizing rate in units of $10^{-13}\ s^{-1}$ per H atom. Reynolds (1986) estimates that in the immediate vicinity of the Sun, a steady-state ionizing rate of ζ_{-13} between 0.4 and 3.0 is required. To produce this range of ionization, the 635 Å intensity we observe would have to be distributed over 7–54% of the sky.

The first soft X-ray background was detected and reported [54] about 25 years ago. Quite naturally, it was assumed that these soft X-ray emissions were from ionized atoms within hot gases. Labov and Bowyer also interpreted the data as emissions from hot gases. However, the authors left the door open for some other interpretation with the following statement from their introduction:

> It is now generally believed that this diffuse soft X-ray background is produced by a high-temperature component of the interstellar medium. However, evidence of the thermal nature of this emission is indirect in that it is based not on observations of line emission, but on indirect evidence that no plausible non-thermal mechanism has been suggested which does not conflict with some component of the observational evidence.

The authors also state that "if this interpretation is correct, gas at several temperatures is present". Specifically, emissions were attributed to gases in three ranges: $5.5 < \log T < 5.7$; $\log T = 6$; $6.6 < \log T < 6.8$.

The explanation proposed herein of the observed dark interstellar medium spectrum hinges on the possibility of energy states below the $n = 1$ state, as given by Eqs. (2a) and (3). A number of experimental observations discussed in Section 1.2 lead to the conclusion that atomic hydrogen can exist in fractional quantum states that are at lower energies than the traditional "ground" ($n = 1$) state. The existence of fractional quantum states of hydrogen atoms explains the spectral observations of the extreme ultraviolet background emission from interstellar space [53], which may characterize dark matter as demonstrated in Table 3. (In these cases, a hydrogen atom in a fractional quantum state, $H(n_i)$, collides, for example, with a $n = \frac{1}{2}$ hydrogen atom, $H(\frac{1}{2})$, and the result is an even lower-energy hydrogen atom, $H(n_f)$, and $H(\frac{1}{2})$ is ionized.

$$H(n_i) + H(\tfrac{1}{2}) \rightarrow H(n_f) + H^+ + e^- + \text{photon}. \qquad (55)$$

The energy released, as a photon, is the difference between the energies of the initial and final states given by Eqs. (2a) and (3) minus the ionization energy of $H(\frac{1}{2})$, 54.4 eV.

Thus, lower-energy transitions of the type

$$\Delta E = \left(\frac{1}{n_f^2} - \frac{1}{n_i^2}\right) 13.6 - 54.4\ \text{eV} \quad n = 1, \frac{1}{2}, \frac{1}{3}, \frac{1}{4}, \cdots$$

$$\text{and} \quad n_i > n_f \qquad (56)$$

Table 2
Energies (Eq. (56)) of several fractional-state transitions catalyzed by $H[a_H/2]$

n_i	n_f	ΔE (eV)	λ (Å)
$\frac{1}{2}$	$\frac{1}{3}$	13.6	912
$\frac{1}{3}$	$\frac{1}{4}$	40.80	303.9
$\frac{1}{4}$	$\frac{1}{5}$	68.00	182.4
$\frac{1}{5}$	$\frac{1}{6}$	95.20	130.2
$\frac{1}{6}$	$\frac{1}{7}$	122.4	101.3
$\frac{1}{7}$	$\frac{1}{8}$	149.6	82.9

induced by a disproportionation reaction with $H[\frac{a_H}{2}]$ ought to occur. The wavelength is related to ΔE by

$$\lambda\ (\text{in Å}) = \frac{1.240 \times 10^4}{\Delta E\ (\text{in eV})}. \qquad (57)$$

The energies and wavelengths of several of these proposed transitions are shown in Table 2. Note that the lower-energy transitions are in the soft X-ray region.

3.2.2. *The data and its interpretation*

In their analysis of the data, Labov and Bowyer [53] established several tests to separate emission features from the background. There were seven features (peaks) that passed their criteria. The wavelengths and other aspects of these peaks are shown in Table 3. Peaks 2 and 5 were interpreted by Labov and Bowyer as instrumental second-order images of peaks 4 and 7, respectively. Peak 3, the strongest feature, is clearly a helium resonance line: He ($1s^1 2p^1 \rightarrow 1s^2$). At issue here, is the interpretation of peaks 1, 4, 6, and 7. It is proposed that peaks 4, 6, and 7 arise from the $\frac{1}{3} \rightarrow \frac{1}{4}$, $\frac{1}{4} \rightarrow \frac{1}{5}$, and $\frac{1}{6} \rightarrow \frac{1}{7}$ hydrogen atoms transitions given by Eq. (55). It is also proposed that peak 1 arises from inelastic helium scattering of peak 4. That is, the $\frac{1}{3} \rightarrow \frac{1}{4}$ transition yields a 40.8 eV photon (303.9 Å). Conspicuously absent is the 256 Å (48.3 eV) line of He II which eliminates the assignment of the majority of the 303 Å line to the He II transition. When this photon strikes He ($1s^2$), 21.2 eV is absorbed in the excitation to He ($1s^1 2p^1$). This leaves a 19.6 eV photon (632.6 Å), peak 1. For these four peaks, the agreement between the predicted values (Table 2) and the experimental values (Table 3) is remarkable.

One argument against this new interpretation of the data is that the transition $\frac{1}{5} \rightarrow \frac{1}{6}$ is missing — predicted at 130.2 Å by Eqs. (56)–(57). This missing peak cannot be explained into existence, but a reasonable rationale can be provided as to why it might be missing from these data. The data obtained by Labov and Bowyer are outstanding

Table 3
Emission features of the Labov and Bowyer spectrum and their interpretation

Peak	λ (Å)	Confidence limit (Å)	Intensity photons $cm^{-2} s^{-1} sr^{-1}$	Assignment (Labov and Bowyer)	Assignment (Mills)	Predicted λ (Eq. (56), (57)) (Å)
1	633.0	−4.7 to +4.7	19,000	O^{4+}; Log $T = 5.5$	He scattering of 303.9 line (peak 4)	633.0
2	607.5	−4.9 to +4.9	Second order	Second order of 302.5 line	Second order of 303.9 line	607.8
3	584	−4.5 to +4.5	70,400	He resonance ($1s^1 2p^1 \rightarrow 1s^2$)	He resonance ($1s^1 2p^1 \rightarrow 1s^2$)	584
4	302.5	−6.0 to +5.9	2080	He^+; ($2p^1$ to $1s^1$)	$n = 1/3$ to $n = 1/4$	303.9
5	200.6	−4.4 to +5.3	Second order	Second order of 101.5 line	Second order of 101.3 line	202.6
6	181.7	−4.6 to +5.1	1030	Fe^{9+} and Fe^{10+}; Log $T = 6$	$n = 1/4$ to $n = 1/5$	182.3
7	101.5	−5.3 to +4.2	790	Fe^{17+} and Fe^{18+}; Log $T = 6.6$–6.8	$n = 1/6$ to $n = 1/7$	101.3

Table 4
Data (Labov and Bowyer) near the predicted $\frac{1}{5} \rightarrow \frac{1}{6}$ transition (130.2 Å)

λ (Å)	Counts	Back ground	Counts-background
125.82	26	21.58	4.42
127.10	22	21.32	0.68
128.37	18	19.50	−1.50
129.64	29	20.28	8.72
130.90	18	19.76	−1.76
132.15	20	19.50	0.50
133.41	19	19.50	−0.50
134.65	19	20.80	−1.80

when the region of the spectrum, the time allotted for data collection, and the logistics are considered. Nonetheless, it is clear that the signal-to-noise ratio is low and that considerable effort had to be expended to differentiate emission features from the background. This particular peak, $\frac{1}{5} \rightarrow \frac{1}{6}$, is likely to be only slightly stronger than the $\frac{1}{6} \rightarrow \frac{1}{7}$ peak (the intensities, Table 3, appear to decrease as n decreases), which has low intensity. Labov and Bowyer provided their data (wavelength, count, count error, background, and background error). The counts minus background values for the region of interest, 130.2 ± 5 Å, are shown in Table 4 (the confidence limits for the wavelength of about ±5 Å are the single-side 1 confidence levels and include both the uncertainties in the fitting procedure and uncertainties in the wavelength calibration). Note that the largest peak (count-background) is at 129.64 Å and has a *counts-background* = 8.72. The *counts-background* for the strongest signal of the other hydrino transitions are: $n = 1/3$–$1/4$, 20.05; $n = 1/4$–$1/5$, 11.36; $n = 1/6$–$1/7$, 10.40. Thus, there is fair agreement with the wavelength and the strength of the signal. This, of course, does not mean that there is a peak at 130.2 Å. However, it is not unreasonable to conclude that a spectrum with a better signal-to-noise ratio might uncover the missing peak. With the assignment of the $\frac{1}{5} \rightarrow \frac{1}{6}$ transition, all of the hydrogen transitions $\frac{1}{3} \rightarrow \frac{1}{4}$, $\frac{1}{4} \rightarrow \frac{1}{5}$, $\frac{1}{5} \rightarrow \frac{1}{6}$, and $\frac{1}{6} \rightarrow \frac{1}{7}$ are observed over the recorded spectral range, and the 632.6 Å peak is identified.

3.3. Identification of lower-energy hydrogen by soft X-rays from the sun

3.3.1. Solar neutrino problem

Another cosmological mystery unresolved for three decades is the discrepancy between solar neutrino flux observed with the Homestake detector, 2.1 ± 0.03SNU, and that predicted based on conservative predictions of the standard solar model (SSM), 7.9 ± 2.6SNU [55–57]. According to the SSM, the pp chain is the predominant energy source of main-sequence stars which commences with proton–proton fusion according to the following reaction [55];

$$^1H + {}^1H \rightarrow {}^2H + e^+ + \nu_e \quad (58)$$

and, according to this model, strong coupling exists between luminosity and neutrino flux because they are both based

on nuclear reactions. An experiment with a radioactive solar surrogate at the Gallex solar neutrino detector in Italy performed over 15 years ago supports the results that over the preceding several years the Gallex and Russia's SAGE, the other large gallium detector, saw only about 60% of the solar neutrino signal predicted to within 1–2% by astrophysical models [58]. The Homestake experiment detects the neutrinos from the pp chain indirectly by detecting ^{8}B neutrinos. A direct measure of neutrinos from the pp chain provides a more definitive test of the SSM. Historically, GALLEX and SAGE were the only two experiments which directly detected electron neutrinos from the pp chain. Recently, GALLEX was upgraded and recommissioned as the Gallium Neutrino Observatory (GNO) which also directly detects pp chain neutrinos to test the deficit observed by GALLEX and SAGE [59–66]. The most recent results from all three experiments show a 50% discrepancy [59–66] which confirms the paradox observed by the Homestake experiment (GNO $65.8^{+10.7}_{-10.2}$SNU [65], GALLEX $74.1^{+6.7}_{-6.8}$SNU [65], SAGE $75.4^{+7.0}_{-6.8}$SNU [61], SSM theoretical 129^{+8}_{-6}SNU [61,66]). Furthermore, Super-Kamiokande operated since 1996 which detects ^{8}B neutrinos by electron scattering (ES) on ordinary water and the recently commissioned Sudbury Neutrino Observatory [67,68] which detects ^{8}B neutrinos by charge current (CC) reaction on deuterium and electron scattering (ES) also reproduced the deficit observed by Homestake (Sudbury $1.75 \pm 0.07\,(\text{stat.})^{+0.12}_{-0.11}$ (sys.) $\pm$ 0.05 (theor.) $\times 10^6\,\text{cm}^{-2}\,\text{s}^{-1}$ (CC) where the theoretical uncertainty is the CC cross-section uncertainty and $2.39 \pm 0.34\,(\text{stat.})^{+0.16}_{-0.14}$ (sys.) $\times 10^6\,\text{cm}^{-2}\,\text{s}^{-1}$ (ES) [67], Super-Kamiokande $2.32 \pm 0.03\,(\text{stat.})^{+0.08}_{-0.07}$(sys.)SNU (ES) [67], SSM theoretical $5.05 \times 10^6\,\text{cm}^{-2}\,\text{s}^{-1}$ [67]).

The recent results from different neutrino detectors around the world all show that the observed solar neutrino flux is only about 34–50% of that predicted. *There is unequivocally a solar neutrino paradox that is directly observable.* Assuming the experiments are accurate within large margins for error (50% or greater), the explanations are: (1) a problem with the standard solar model and (2) neutrino oscillation. However, oscillation violates the standard model — it does not conserve family Lepton number and requires a neutrino mass different from zero [64]. Furthermore, if neutrinos oscillate, then the universe should be full of tau neutrinos which were once proposed as the identity of dark matter. But, a detailed search for signature emissions has yielded nil [49]. Neutrino oscillation has never been directly observed. The Sudbury [67] results showed no evidence for a deviation of the spectral shape from the predicted shape under the non-oscillation hypothesis. In addition, the precise measurement of the spectrum shape and day/night fluxes measured by Super-Kamiokande does not show evidence of neutrino oscillation [69,70].

The paradox of the paucity of solar neutrinos to account for the solar energy output by the pp chain is resolved by assigning a major portion of the solar output to hydrogen transitions. Hydrogen transitions to electronic energy levels below the "ground" state corresponding to fractional quantum numbers can yield energies comparable to nuclear energies. For example, all transitions to the $n = \frac{1}{100}$ state of hydrogen taken together release 136 keV. Data strongly supporting this tenant is the observation by Labov and Bowyer of an intense 304 Å (40.8 eV) solar emission line corresponding to the transition given by Eq. (55)

$$H\left[\frac{a_H}{3}\right] \xrightarrow{H[a_H/2]} H\left[\frac{a_H}{4}\right] \tag{59}$$

in the absence of the 256 Å (48.3 eV) line of He II which challenges the assignment of the 304 Å line to the He II transition. Solar lines which match lower-energy hydrogen transitions shown in Table 5 are also observed on the Sun which is consistent with a stellar origin of lower-energy hydrogen in interstellar space.

3.3.2. *Temperature of the solar corona problem*

In addition to the questions of what powers the Sun and why the solar neutrino flux is significantly deficient, there exists no satisfactory answer to two additional solar questions: The cause of sunspots and other solar activity and why the Sun emits X-rays is unknown [75]. In fact, a possible anticorrelation exists between the abundance of sunspots and the solar neutrino flux observed with the Homestake detector [76]. The photosphere of the Sun is 6000 K; whereas, the temperature of the corona based on the assignment of the emitted X-rays to highly ionized heavy elements is in excess of 10^6 K. No satisfactory power transfer mechanism is known which explains the excessive temperature of the corona relative to that of the photosphere. The mechanism must explain the constant transfer over time of energy from the photosphere at 6000 K to the corona at 10^6 K which radiates energy into cold space. Further compounding the temperature mystery is the observation of a strong coronal hydrogen Lyman series, beginning with Lx at 1216 Å and ending at 912 Å, corresponding to unionized hydrogen atoms. The hydrogen lines would indicate that the corona is less than 10^4 K. The paradox is resolved by the existence of a power source associated with the corona.

The cause of sunspots and other solar activity, and why the Sun emits X-rays can be explained by energy releasing transitions of hydrogen to lower-energy levels. The energy which maintains the corona at a temperature that appears in excess of 10^6 K may be that released by disproportionation reactions of lower-energy hydrogen as given by Eqs. (10)–(12). Hydrogen transitions to electronic energy levels below the "ground" state corresponding to fractional quantum numbers match lines of the solar emission spectrum in the extreme ultraviolet and X-ray regions. The solar lines that match the energy of disproportionation reactions of lower-energy hydrogen given by Eqs. (10)–(12) are given in Table 5.

Table 5
Observed solar line emission assigned to the disproportionation reactions given by Eqs. (10)–(12). (Raw extreme ultraviolet solar spectral data taken from Figs. 3a–k of [71], Figs. 1a–d (observed lines from Table 1) of [72]; Fig. 7.5 of [73], and Fig. 4.10 of Phillips [74].)

Observed line (Å)	Predicted (Mills)[b] (Å)	m, m'	Assignment (Mills)	Ref	Assignment (Other)
1215.7	1215.67	[d]	$H(2p^1) \rightarrow H(1s^1) + 10.2$ eV	[73,74]	Collisional excitation, $L\alpha$ scattering
911.8	911.78	1, 1;1[c]	1 → 1/2 H transition	[73,74]	$H^+ + e^- \rightarrow H + 13.6$ eV at $T > 20,000$ K
		1, 2	1/2 → 1/3 H transition		
584.5	584.5	[c]	$He(1s^1 2p^1) \rightarrow He(1s^2) + 21.2$ eV	[73,74]	Collisional excitation
373.7	373.73	2, 2	Inelastic scattering (He) of 1 → 1/3 H transition	[71]	None
303.8	303.92	1, 2	1/3 → 1/4 transition	[71]	He II
280.2[a] 280.8[a]	280.54	2, 2	Inelastic scattering (H) of 1 → 1/3 H transition	[72]	None
264.80	265.08	1, 2	Inelastic scattering (He) of 1/4 → 1/5 H transition	[72]	Fe XIV
228[a]	227.95	2, 2	1 → 1/3 H transition	[72]	None
215.16	214.54	1, 2	Inelastic scattering (H) of 1/4 → 1/5 H transition	[72]	S XII
182.16	182.36	1, 2	1/4 → 1/5 H transition	[72]	Fe XI
167.50	167.62	1, 2	Inelastic scattering (He) of 1/5 → 1/6 H transition	[72]	Fe VIII
152.15	151.97	3, 3	1 → 1/4 H transition	[72]	Ni XII
145.9[a]	145.88	1, 2	Inelastic scattering (H) of 1/5 → 1/6 H transition	[72]	None
141[a]	141.59	2, 2	Inelastic scattering (He) of 1/2 → 1/4 H transition	[72]	None
129.87	130.26	1, 2	1/5 → 1/6 H transition	[72]	O VI
125.5a	125.76	2, 2	Inelastic scattering (H) of 1/2 → 1/4 H transition	[72]	None
122.2[a]	122.56	1, 2	Inelastic scattering (He) of 1/6 → 1/7 H transition	[72]	None
114[a]	113.97	2, 2	1/2 → 1/4 H transition	[72]	None
110.5[a]	110.52	1, 2	Inelastic scattering (H) of 1/6 → 1/7 H transition	[72]	None
101.3[a]	101.31	1, 2	1/6 → 1/7 H transition	[72]	None
96.7[a]	96.59	1, 2	Inelastic scattering (He) of 1/7 → 1/8 H transition	[72]	None
88.8	88.95	1, 2	Inelastic scattering (H) of 1/7 → 1/8 H transition	[72]	None
87.0[a]	87.34	2, 2	Inelastic scattering (He) of 1/3 → 1/5 H transition	[72]	None
82.9[a]	82.89	1, 2	1/7 → 1/8 H transition	[72]	None
81.1[a]	81.05	2, 2	Inelastic scattering (H) of 1/3 → 1/5 H transition	[72]	None
79.58	79.70	1, 2	Inelastic scattering (He) of 1/8 → 1/9 H transition	[72]	Fe XII
76.0[a]	75.98	2, 2	1/3 → 1/5 H transition	[72]	None
70.1[a]	70.14	1, 2	1/8 → 1/9 H transition	[72]	None
67.5[a]	67.84	1, 2	Inelastic scattering (He) of 1/9 → 1/10 H transition	[72]	None
63.12	63.14	2, 2	Inelastic scattering (He) of 1/4 → 1/6 H transition	[72]	Mg X

Table 5. (*Continued*).

Observed line (Å)	Predicted (Mills)[b] (Å)	m, m'	Assignment (Mills)	Ref	Assignment (Other)
61.0[a]	60.78	1, 2	1/9 → 1/10 H transition	[72]	None
59.7[d]	59.79	2, 2	Inelastic scattering (H) of 1/4 → 1/6 H transition	[72]	None

[a]Wavelength read from Fig. 1 of [72]; wavelength not given in Table of [72].

[b]For lower-energy transitions, $n = 1, \frac{1}{2}, \frac{1}{3}, \frac{1}{4}, \ldots$, and $n_i > n_f$ induced by a disproportionation reaction with $H[a_H/2]$, $E = (1/n_f^2 - 1/n_i^2)13.6\ \text{eV} - m'^2 13.6\ \text{eV}$. For helium inelastic scattered peaks of hydrogen transitions, $n_i \rightarrow n_f$, $E = (1/n_f^2 - 1/n_i^2)13.6\ \text{eV} - m'^2 13.6 - 21.21\ \text{eV}$ (when this photon strikes He ($1s^2$), 21.2 eV is absorbed in the excitation to He ($1s^1 2p^1$)). For hydrogen inelastic scattered peaks of hydrogen transitions, $n_i \rightarrow n_f$, $E = (1/n_f^2 - 1/n_i^2)13.6\ \text{eV} - m'^2 13.6 - 10.2\ \text{eV}$ (when this photon strikes H ($1s^1$), 10.2 eV is absorbed in the excitation to H($2p^1$)).

[c]$H\ [n = 1] \overset{2H}{\rightarrow} H\ [n = \frac{1}{2}] + h\nu$ (911.8 Å).

[d]$H\ (2p^1) \rightarrow H\ (1s^1) + 10.2\ \text{eV}$ (excitation by emission of lower-energy hydrogen transitions).

[e]$He\ (1s^1 2p^1) \rightarrow He\ (1s^2) + 21.2\ \text{eV}$ (excitation by emission of lower-energy hydrogen transitions).

[f]Eqs. (10)–(12).

The agreement between the calculated and the experimental values is remarkable, and several match those identified by EUV spectroscopy of the helium–hydrogen plasma as shown in Table 1. Furthermore, many of the lines of Table 5 had no previous assignment, or the assignment was unsatisfactory. Some lines assigned in the literature may have been assigned incorrectly by trying to fit the spectrum to known lines. But, inconsistencies arise. For example, the intensity of the peak assigned to He II by Thomas [71] is extremely strong ($I = 62,200$). The laboratory He II transition intensities are: $I(303.780) = 1000$; $I(303.786) = 500$; $I(256) = 300$. Therefore, the predicted peak intensity of the 256 Å (48.3 eV) line of He II is $I = 12,440$; whereas, the observed intensity is too weak ($I = 1580$) which challenges the assignment of the 304 Å line solely to the He II transition.

Temporal variation in the disproportionation line intensities may reflect solar activity. For example, the coronal power is $\cong$ 0.01% of the solar power in the case of a quite Sun and as high as 100% of the solar power in the case of an active Sun [77]. Emission lines corresponding to lower-energy hydrogen transitions and assigned as such in Table 5 greatly increase in intensity during flare events [1,78–80] which is evidence that lower-energy hydrogen transitions may be a factor in the cause of solar flares.

4. Conclusion

Transitions to fractional quantum energy levels were previously recorded at the Institut für Niedertemperatur-Plasmaphysik e.V. We report that extreme ultraviolet (EUV) spectroscopy was recorded on microwave and glow discharges of helium with 2% hydrogen. Novel emission lines were observed with energies of $q13.6$ eV where $q = 1,2,3,4,6,7,8,9$, *or* 11 or these lines inelastically scattered by helium atoms wherein 21.2 eV was absorbed in the excitation of He ($1s^2$) to He ($1s^1 2p^1$). These lines were identified as hydrogen transitions to electronic energy levels below the "ground" state corresponding to fractional quantum numbers. Furthermore, astrophysical data was reviewed, and such transitions were found to match the spectral lines of the extreme ultraviolet background of interstellar space. These transitions may resolve the paradox of the identity of dark matter and account for many celestial observations such as: diffuse Hα emission is ubiquitous throughout the Galaxy and widespread sources of flux shortward of 912 Å are required. The origin of the 633 Å emission observed by Labov and others [53] that could be a major source of ionization of interstellar hydrogen was also observed in our helium–hydrogen plasma. We assigned the 633 Å emission to atomic helium scattered 304 Å emission from the $H[a_H/3] \overset{H[a_H/2]}{\rightarrow} [a_H/4]$ hydrogen transition.

Furthermore, fractional hydrogen transitions were also assigned to lines in the solar EUV spectrum which may resolve the solar neutrino problem, the mystery of the cause of sunspots and other solar activity, and why the Sun emits X-rays. In addition to producing power on the Sun, the catalysis of hydrogen represents a new powerful energy source with the potential for direct conversion of plasma to electricity with the production of novel compounds [40,41].

Acknowledgements

Special thanks to Y. Lu and T. Onuma for recording some spectra and B. Dhandapani for assisting with logistics and reviewing this manuscript. Special thanks to S. Labov and S. Bowyer for providing their raw digitized spectroscopic data and W. Good for bringing this paper to my attention. Special thanks to J. Farrell for contributions to the analysis of the interstellar and solar spectral data.

References

[1] Mills R. The grand unified theory of classical quantum mechanics, January 2000 edn. Cranbury, NJ: BlackLight Power, Inc, Distributed by Amazon.com.

[2] Mills R. The grand unified theory of classical quantum mechanics. Global foundation, Inc. Orbis Scientiae entitled The Role of Attractive and Repulsive Gravitational Forces in Cosmic Acceleration of Particles The Origin of the Cosmic Gamma Ray Bursts, 29th Conference on High Energy Physics and Cosmology Since 1964, Dr. Behram N. Kursunoglu, Chairman, December 14–17, 2000, Lago Mar Resort, Fort Lauderdale, FL.

[3] Mills R. The grand unified theory of classical quantum mechanics. Global Foundation, Inc. Orbis Scientiae entitled The Role of Attractive and Repulsive Gravitational Forces in Cosmic Acceleration of Particles The Origin of the Cosmic Gamma Ray Bursts, 29th Conference on High Energy Physics and Cosmology Since 1964, Dr. Behram N. Kursunoglu, Chairman, Lago Mar Resort, Fort Lauderdale, FL, New York: Kluwer Academic/Plenum Publishers, December 14–17, 2000. p. 243–58.

[4] Mills R. The grand unified theory of classical quantum mechanics. Int J Hydrogen Energy, in press.

[5] Mills R. The hydrogen atom revisited. Int J Hydrogen Energy 2000;25(12):1171–83.

[6] Mills R. The nature of free electrons in superfluid helium — a test of quantum mechanics and a basis to review its foundations and make a comparison to classical theory. Int J Hydrogen Energy 2001;26(10):1059–96.

[7] Mills R, Ray P. Vibrational spectral emission of fractional-principal-quantum-energy-level hydrogen molecular ion. Int J Hydrogen Energy, in press.

[8] Mills R, Ray P. Spectroscopic identification of a novel catalytic reaction of potassium and atomic hydrogen and the hydride ion product. Int J Hydrogen Energy, in press.

[9] Mills R. Spectroscopic identification of a novel catalytic reaction of atomic hydrogen and the hydride ion product. Int J Hydrogen Energy 2001;26(10):1041–58.

[10] Mills R, Greenig N, Hicks S. Optically measured power balances of anomalous discharges of mixtures of argon, hydrogen, and potassium, rubidium, cesium, or strontium vapor. Int J Hydrogen Energy, submitted for publication.

[11] Mills R, Nansteel M. Argon–hydrogen–strontium plasma light source. IEEE Trans Plasma Sci, submitted for publication.

[12] Mills R, Nansteel M, Lu Y. Excessively bright hydrogen–strontium plasma light source due to energy resonance of strontium with hydrogen. European J Phys D, submitted for publication.

[13] Mills R, Dong J, Lu Y. Observation of extreme ultraviolet hydrogen emission from incandescently heated hydrogen gas with certain catalysts. Int J Hydrogen Energy 2000;25: 919–43.

[14] Mills R. Observation of extreme ultraviolet emission from hydrogen-KI plasmas produced by a hollow cathode discharge. Int J Hydrogen Energy 2001;26(6):579–92.

[15] Mills R. Temporal behavior of light-emission in the visible spectral range from a Ti-K2CO3-H-Cell. Int J Hydrogen Energy 2001;26(4):327–32.

[16] Mills R, Onuma T, Lu Y. Formation of a hydrogen plasma from an incandescently heated hydrogen-catalyst gas mixture with an anomalous afterglow duration. Int J Hydrogen Energy 2001;26(7):749–62.

[17] Mills R, Nansteel M, Lu Y. Observation of extreme ultraviolet hydrogen emission from incandescently heated hydrogen gas with strontium that produced an anomalous optically measured power balance. Int J Hydrogen Energy 2001;26(4): 309–26.

[18] Mills R, Dong J, Lu Y, Conrads J. Observation of extreme ultraviolet hydrogen emission from incandescently heated hydrogen gas with certain catalysts. 1999 Pacific Conference on Chemistry and Spectroscopy and the 35th ACS Western Regional Meeting, Ontario Convention Center, California, October 6–8, 1999.

[19] Mills R, Dong J, Greenig N, Lu Y. Observation of extreme ultraviolet hydrogen emission from incandescently heated hydrogen gas with certain catalysts. 11th Annual US Hydrogen Meeting, Vienna, VA, National Hydrogen Association, February 29–March 2, 2000.

[20] Mills R, Dhandapani B, Greenig N, He J, Dong J, Lu Y, Conrads H. Formation of an energetic plasma and novel hydrides from incandescently heated hydrogen gas with certain catalysts. 11th Annual US Hydrogen Meeting, Vienna, VA, National Hydrogen Association, February 29–March 2, 2000.

[21] Mills R, Dong J, Greenig N, Lu Y. Observation of extreme ultraviolet hydrogen emission from incandescently heated hydrogen gas with certain catalysts. 219th National ACS Meeting, San Francisco, CA, March 26–30, 2000.

[22] Mills R, Dhandapani B, Greenig N, He J, Dong J, Lu Y, Conrads H. Formation of an energetic plasma and novel hydrides from incandescently heated hydrogen gas with certain catalysts. 219th National ACS Meeting, San Francisco, CA, March 26–30, 2000.

[23] Mills R, Dhandapani B, Greenig N, He J, Dong J, Lu Y, Conrads H. Formation of an energetic plasma and novel hydrides from incandescently heated hydrogen gas with certain catalysts. 29th Northeast Regional Meeting, University of Connecticut, Storrs, CT, June 18–21, 2000.

[24] Mills R, Dhandapani B, Greenig N, He J, Dong J, Lu Y, Conrads H. Formation of an energetic plasma and novel hydrides from incandescently heated hydrogen gas with certain catalysts. 220th ACS National Meeting, Washington, DC, August 20–24, 2000.

[25] Mills R, Dhandapani B, Nansteel M, He J, Voigt A. Identification of compounds containing novel hydride ions by nuclear magnetic resonance spectroscopy. Int J Hydrogen Energy 2001;26(9):965–79.

[26] Mills R, Dhandapani B, Greenig N, He J. Synthesis and characterization of potassium iodo hydride. Int J Hydrogen Energy 2000;25(12):1185–203.

[27] Mills R. Novel inorganic hydride. Int J Hydrogen Energy 2000;25:669–83.

[28] Mills R. Novel hydrogen compounds from a potassium carbonate electrolytic cell. Fusion Technol 2000;37(2):157–82.

[29] Mills R, Dhandapani B, Nansteel M, He J, Shannon T, Echezuria A. Synthesis and characterization of novel hydride compounds. Int J Hydrogen Energy 2001;26(4): 339–67.

[30] Mills R. Highly stable novel inorganic hydrides. J New Mat Electro Syst, submitted for publication.

[31] Mills R. Novel hydride compound. 1999 Pacific Conference on Chemistry and Spectroscopy and the 35th ACS Western